1-1-2014

Facile Fabrication Of Mesostructured Zn2sno4 Based Anode Materials For Reversible Lithium Ion Storage

Sai Karthik Karthik Addu
Wayne State University,

FACILE FABRICATION OF MESOSTRUCTURED Zn_2SnO_4 BASED ANODE MATERIALS FOR REVERSIBLE LITHIUM ION STORAGE

by

SAI KARTHIK ADDU

THESIS

Submitted to the Graduate School

of Wayne State University,

Detroit, Michigan

in partial fulfillment of the requirements

for the degree of

MASTER OF SCIENCE

2014

MAJOR: CHEMICAL ENGINEERING

Approved By:

_____

Advisor   Date

DEDICATION

To,

My family

ACKNOWLEDGMENTS

Firstly, I want to thank my advisor, Dr Da Deng for giving me the privilege to do research for my master thesis and the unique research opportunity. He has always been there to support my research and provide me invaluable guidance over the last two semesters while I was working on this master thesis. I gratefully appreciate his help and time out of his busy schedule. His creative thinking, attentions to scientific details, constructive criticisms and insightful comments has greatly helped me to form this thesis. His dedication and enthusiasm for scientific research and novel ideas across different disciplines have always been inspiring. He always has confidence with me and encourages me to do good science and challenge the existing paradigms. He has helped me not only on my research project itself but taught me to carry out a good research experiments, how to write a thesis and properly cite literature. He always encourages me to be my best.

I would also like to thank my colleagues Jian Zhu, Xianghua and Wei Chen all of them have helped me and played an important role in my work. I would also like to thank my friend Ayad Nacy for supporting me all the way.

I would like to deeply thank my family and friends in USA and India, for always being there for me and for supporting me in whatever I do.

TABLE OF CONTENTS

LIST OF TABLES

LIST OF FIGURES

Chapter 1 Introduction

1.1 Objectives

Today's energy economy is based so much on fossil fuels which has problems like being a non-renewable resource and then there is great demand for these resources as never before i.e. high demand for oil and these are produced from politically unstable countries which compounds to the problem even more. Add to it the carbon dioxide produced from these fuels have almost doubled from 1970's and pose a huge problem to climate-change[5].

The solution for these problems has been renewable energy resources which are ecological friendly, low-cost and serve for long term. These include solar, wind and the biofuels. Battery systems can be used to store this renewable energy. Batteries have lot have advantages and are highly important part of the renewable resources plan. The performance of the batteries depends mostly on the properties of their materials. New material chemistry has already made advances in the energy conversion and storage field. Lithium-ion batteries have been replacing lead-acid and nickel-metal hydride batteries for the last few years.

One needs to look at the recent developments in electric-cars and hybrid vehicles to understand the relevance of Lithium-ion batteries in the market. These are being used by all the major electric car makers and promise customers the reliability and safety of the electric cars. The other important market for batteries has been the electronics market such as Smartphone's and robotics which use batteries in them. These technological improvements demand for higher energy density and power and not to forget the cyclability of the batteries.

Lithium-ion batteries have more than 2500 cycles, can be made into different sizes and also require very little maintenance compared to the other battery technologies. Different ways are being researched to make Lithium-ion batteries more cost efficient and improve its cycling life and last but not the least increase its safety. Additionally, Lithium-ion batteries can be employed to buffer green but fluctuating energy sources, such as wind and solar energy. The combination of Lithium-ion batteries and green energy will offer reliable smart energy source at supply-on-demand model achieving high energy efficiency. Figure 1 clearly shows the advantages of Lithium-ion batteries as compared to other rechargeable batteries. Li-based batteries have higher energy density compared to lead-acid, Nickel-cadmium and Nickel-metal hydride.
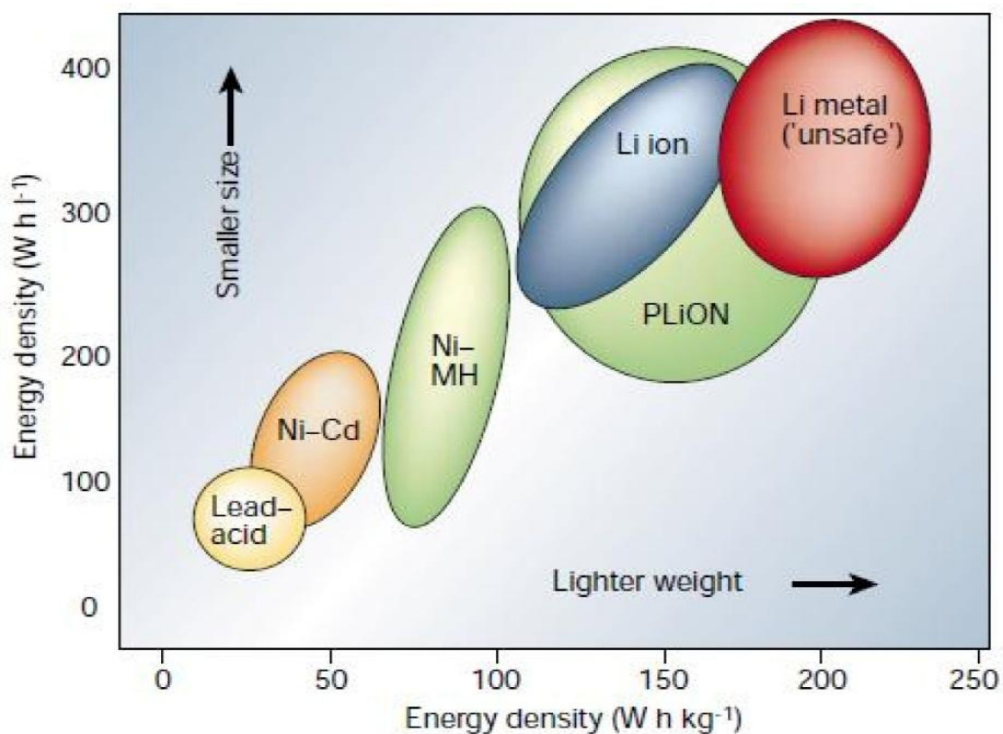
Figure 1: Comparison of various rechargeable battery technologies in terms of energy density[1]

The objectives of this thesis are:

1. To design new mesostructures based anode material compositions which can exhibit higher capacities than that of commercially available carbon anode materials.

2. To synthesize low-cost and environmentally benign Zn_2SnO_4 based anode materials and fully characterize the materials using state-of-the-art techniques.

3. To thoroughly investigate their performance in lithium ion batteries by electrochemical testing and possibly improve the current set of materials being used for Lithium-ion batteries, which are effective but are also expensive and toxic.

In the next 3 chapters I am going to review the current works in anode and cathode materials. Then show the results obtained in our lab for Zn_2SnO_4-based anode materials. Here is an outline of the things in the chapters.

Chapter 2 deals with literature review of the anode and cathode materials and also with the basic ways of working of the batteries and a brief history of the batteries. It also has a separate section in which it deals with carbon coating Chapter 3 deals with carbon coating of the ZTO based cubic material and its performance in battery testing. Chapter 4 deals with Rubik cube-shaped ZTO based anode material and its characterization and electrochemical performance.

Chapter 2 Literature Review

2.1 Basic Principles of lithium Ion Batteries

Lithium batteries use a reductant as the anode and an oxidant as the cathode. Simply put, on discharge the anode supplies Li^+ ions to the Li^+ electrolyte and electrons to the external circuit. Cathode materials take these Li^+ ion coming in from the electrolyte and the charge is balanced by the external circuit. On charge, reversal of this process occurs, that is the Li^+ ions go back to the anode through the electrolyte and into the host structure. The electronic current delivered by the cell is matched by the ionic current inside the cell.

This cell has been called "Rocking-chair" cell as both the anode and cathode act as hosts for the reversible insertion or removal of the ion. Another important part of the battery is the electrolyte which is a form of a solution of a Li salt, specifically, $LiPF_6$ dissolved in a mixture of ethylene carbonate (EC) and diethyl carbonate (DEC), Dimethyl carbonate (DMC), or both. It can also be in the form of a gel such as polyvinylidene fluoride (PVDF). Figure 2 describes a basic Lithium-ion battery diagram showing the Li^+ ions passing through the electrolyte.
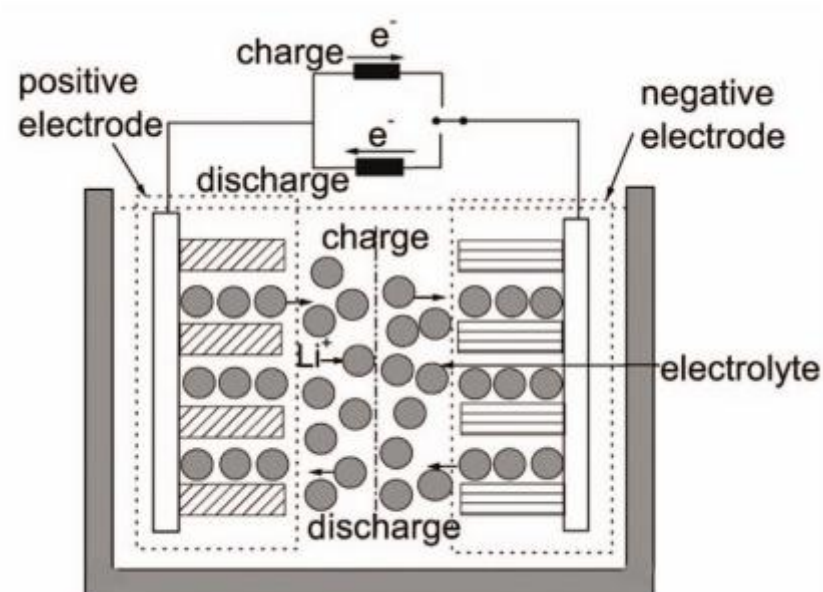
Figure 2: Basic Schematic diagram of a Lithium-ion battery with different electrodes and Li insertion into them[2].

Batteries have come a long way but present-day battery technologies are being outpaced by the ever-increasing power demands from new applications. Batteries today have to be not only safe but they also have to integrate the concept of environmental sustainability. Hence recent developments have been to incorporate newer and hybrid nanomaterials Various nanostructured materials have been developed for Lithium-ion batteries like SnO_2 nanotubes[6], SnO_2 microstructures[7] .Certain level of success has been achieved in improving the performance of Lithium-ion batteries. However, it is still very challenging to prepare nanomaterials with desired structures by a facile method.

2.2 Cathode Materials for Lithium Ion batteries

Compared to anode, the cathode materials have been researched a lot and some of the candidate cathode materials include $LiCoO_2$, Li NiO_2, $LiNi_{1-y}Co_yO_2$ and three-dimensional $LiMn_2O_4$ spinel phase. $LiCoO_2$ has dominated the market since it was commercialized by Sony Corporation in 1991.Because of the high cost and toxicity of cobalt different cathodes has been developed.$LiMn_2O_4$ has been extensively studied as it has many advantages like less toxic and less cost[8]. The olivine $LiFePO_4$ have attracted attention recently for its structure and performance in lithium batteries[9]. Chunwen Sun et al[10] prepared monodisperse porous $LiFePO_4$ microspheres for a high power lithium-ion battery cathode. They used solvothermal with high-temperature calcination to synthesize $LiFePO_4$.

These materials are generally prepared through high temperature calcination with temperature around 800 °C. One of other important factor to be seen in the cathode materials is the phase transformation during intercalation process. They are divided into two categories i.e. a homogeneous solid phase reaction and a two-phase reaction.
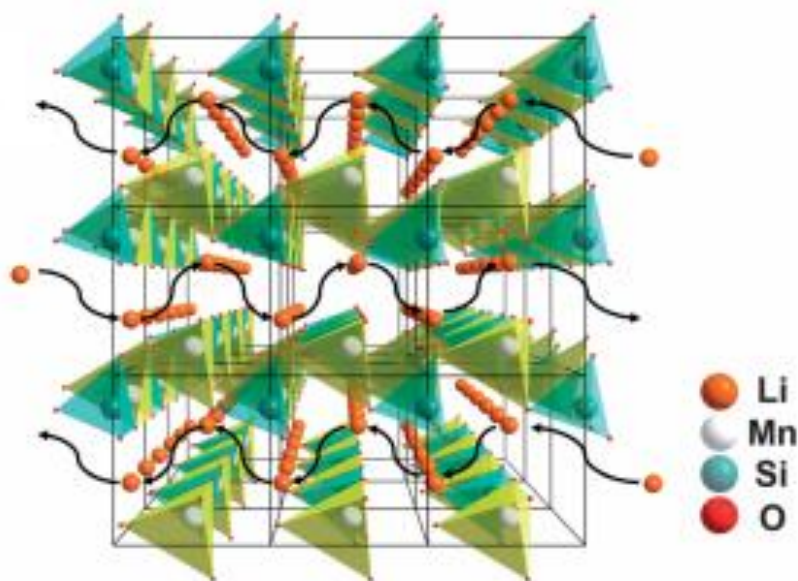
Figure 3: Schematic representation of the structure Li_2MnSiO_4 also showing the Li^+ migration[3].

Zhe et al[3] recently showed the Li_2MnSiO_4 with carbon as nanocomposites as a high capacity cathode material for Lithium-ion battery. These were prepared through the hydrothermal method. The electrochemical measurement showed an initial discharge capacity of 281.5mAh/g.

There are materials which are doped with other transition metals to improve the performance of the cathodes. One such example is of Cr-doped $Li_xMn_{1.5}Ni_{0.5}O_4$ 5-V cathode material[11]. Other researchers have tried to add yttrium content into the cathode material resulting in superior rate capability of the electrode[12].

2.3 Anode Materials for Lithium Ion Batteries

Over the years there has been intensive research in improving the overall performance of Lithium-ion batteries. The energy density of the Lithium-ion batteries depends on the capacities and operating potentials of the respective electrode materials. One of the main ways to improve the batteries has been to improve the anode materials as the graphite anode currently used in Lithium-ion rechargeable batteries has a theoretical capacity of 370mAh/g but the practical capacity that is seen is around 320mAh/g. Thus, there is a need to find electrode materials that can yield higher capacities and high energy density.

Different anode materials like silicon nanorods[13], silicon/carbon composites[14] and germanium/carbon nanostructures[15] have been used as anode materials and have given great results but there is still room for improving the battery performance. Some of the properties of an ideal anode material for Lithium-ion batteries are as follows: (1) It must be a compound with low atomic weight, be low density and accommodate fairly large amounts of Li per formula unit and be cyclable, to yield large, stable and reversible gravimetric (mAh/g) capacities. (2) An ideal anode material should have a potential as close as possible to that of the Li metal as possible. (3) The anode material must not be soluble in the solvents of the electrolyte and must not be chemically react with the salt or solvents of the electrolyte.

2.3.1 Carbon based Anode for Lithium Ion Batteries

Carbon anodes became a breakthrough in realizing the lithium "rocking chair" battery and solved the lithium metal anode safety problem. Carbon attracts lot of interest because of its diverse characteristics such as a variety of structures which plays an important role. Kanno et al[16] reported in 1989 the use of carbon as electrodes and have discussed in detail the importance of surface area. Number of people working on it increased with Sony marketing its first lithium ion battery in 1991. Graphite as active materials has been particularly attractive because of large capacity of lithium intercalation and low average voltage. Simon et al had published on the choice of graphite for lithium ion batteries[17]. Other researchers also worked on using graphite oxide and graphene oxide as electrodes for lithium ion batteries[18]. Graphite has been researched thoroughly and now research is being to explore the unique properties of the graphene. Jung Ji et al[19] recently published graphene-encapsulated Silicon as anode. Silicon has been shown great interest due to its high theoretical capacity (4200 mAh/g). The graphene encapsulated Si nanoparticles were prepared by mixing an aqueous suspension of poly (diallyldimethylammonium chloride) (PDDA) modified Si nanoparticles with a graphene oxide (G-O) aqueous suspension.
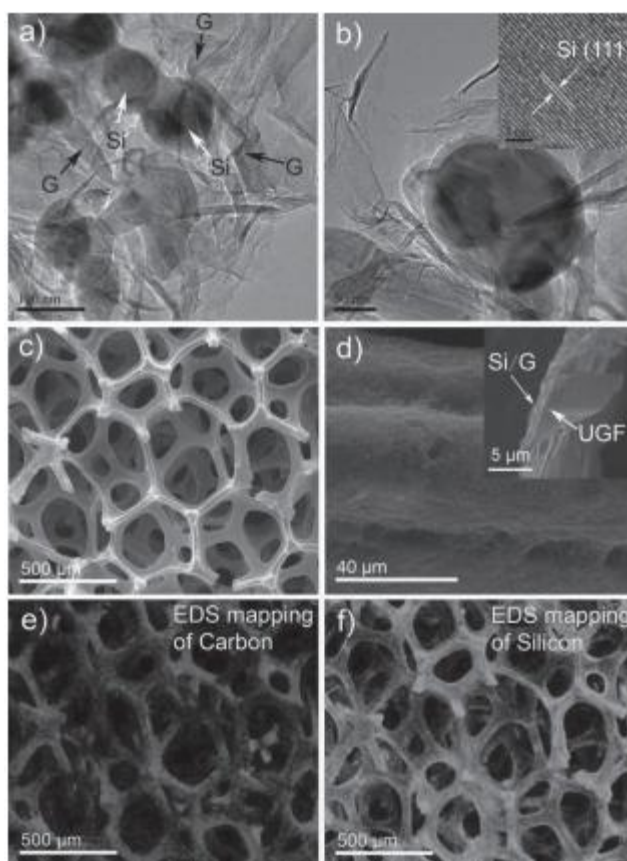
Figure 4: (a,b) TEM images of graphene encapsulated Si,(b) HRTEM of the Si nanoparticles,(c,d) SEM images of the structure(d-inset) cross-sectional view of the composite(e,f) EDS mapping of silicon and carbon[19].

Graphene with its two dimensional carbon material has high electrical conductivity, superior mechanical flexibility and low density. Xiefei Li et al[20] published their research on anode made of nitrogen-doped graphene nanosheet. One of the interesting they showed was specific capacity increased over number of cycles. The specific capacity of 684 mAh g^{-1} in the 501st cycles and 452 mAh g^{-1} in the 100th cycle, which shows higher cycling stability and larger specific capacity in comparison to a pristine graphene and a commercial

graphite anode. The nitrogen-doped graphene nanosheet was made through thermal treatment at 1050°C under nitrogen atmosphere.
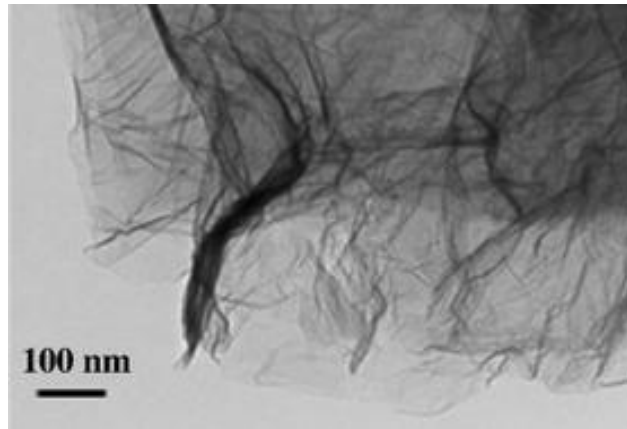
Figure 5: TEM image of the graphene nanosheet which was doped with nitrogen later[20].

2.3.2 Anodes based on Li intercalation –deintercalation reaction

Intercalation basically here means insertion of the ion, atom or molecule into a crystal lattice of a host compound without destroying the crystal structure. Though these don't destroy the host but they do modify the crystal structure. Three important conditions that these compounds should satisfy are[4]: Firstly, the compound must be crystalline and should have empty sites in the host crystal lattice, in the form of isolated vacancies. Compounds with 2D and 3D structures are most useful for Li intercalation-deintercalation whereas compounds with isolated vacant sites or 1D channel may easily intercalate but not easily deintercalate Li ions. Second, the host compound must contain a transition metal or rare earth metals which can exhibit one or more stable valency states. This is because intercalation of Li ion will reduce the valency state of the host metal ion by one unit. The third condition is that if the host compound has an unfavorable crystal structure and transition metals in low valency state, Li intercalation may not occur.

One way of understanding the Li intercalation process has been to understand the key factors that govern Li diffusion in intercalation compounds and illustrate how the complexities of Li diffusion mechanisms work. Anton et al[21] have concluded that Li diffusion coefficient of an intercalation compound is a crucial kinetic parameter that determines how rapidly Li can be removed and reinserted into the compound. They use first principles statistical mechanics approaches can elucidate the effect of chemistry and crystal structure on kinetic properties.

2.3.2.1 Binary Oxides

The most attractive binary oxide has been Titanium dioxide, TiO_2, for use as an anode for Lithium-ion batteries due to its low cost, ready availability, and ecofriendliness. TiO_2 exists in several polymorphic modifications: anatase, rutile, brookite, TiO_2-B (bronze) etc. All of them contain TiO_2 octahedra.
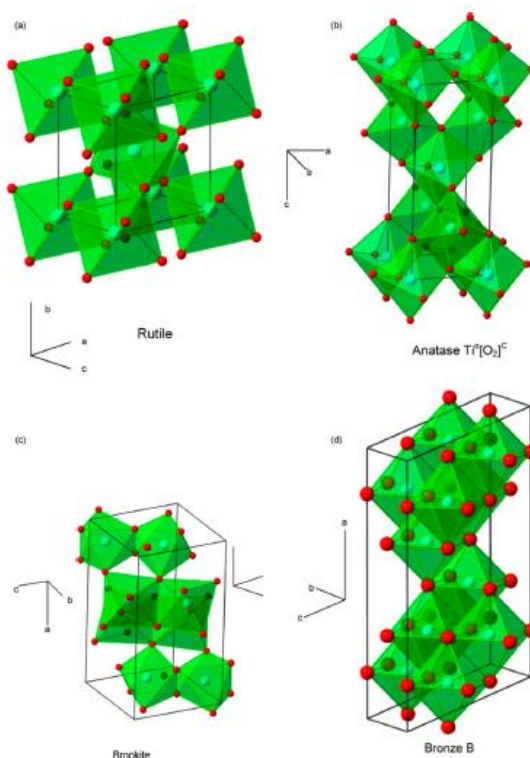
Figure 6: Crystallographic representation of rutile, anatase, brookite and bronze (B) TiO_2[4].

TiO_2 performance mainly depends upon method of preparation of TiO_2, particle size, and shape and morphology. Particles with size less than 200nm with higher surface area and porous morphology with interconnected particles can give stable and near theoretical capacity. Similarly the Vanadium and molybdenum oxides (VO, V_2O_3, VO_2, V_2O_5) have been investigated and have shown to be good anode materials for Lithium-ion batteries.

2.3.2.2 Ternary Oxides

Many ternary titanium and niobium oxides possessing 2D-layer or 3D-network have been examined in the literature for Li-Cyclability, in particular nanostructured forms, have been fabricated and investigated for the applications[22]. One disadvantage that has been found with these is that they have very low electronic conductivity (at 300K, sigma ~ 10^{-9} to 10^{-13} S cm^{-1}).

Lithium titanium oxide ($Li_4Ti_5O_{12}$) with the cubic spinel structure has been investigated for Li storage and cyclability in the form of micro- and nanocrystalline particles and with various morphologies and composites. It has a theoretical value of 175 mAh/g and many have been able to get close to the value. Zhu et al[23] prepared composites of 1 wt% graphene and nano-LTO, which had a surface area of 170 m^2/g, by electro spinning and heat treatment. At 22C, the LTO-graphene composite gave a specific capacity of 110mAh/g.

Jung et al[24] prepared bare and carbon coated LTO by a two-step process involving solid state reaction and pitch carbon. The 5 micrometer sized spherical particles are composed of 100nm sized primary particles, and the nominal 5 wt% C-coated LTO had a uniform 3nm thick carbon coating. While the BET surface areas did not vary much before and after C-coating, the electronic conductivity increased by 6 orders of magnitude in the C-coated LTO.

2.3.3 Metal Oxides Based Anode for Lithium Ion batteries

Elements like Si, Sb and metals like Sn, In and Cd[25] can give rise to Li storage and cycling behavior by virtue of alloying-dealloying reactions. An example of the process can be explained in first discharge reaction with Li, SnO or SnO_2 undergoes crystal structure destruction and formation of nano-Sn metal dispersed in amorphous Li_2O via a two phase reaction. This is followed by alloy formation, $Li_{4.4}Sn$. Detailed studies have shown that Li alloying-dealloying reactions of Sn,Si,Sb etc. involve large changes in the unit cell volume, as high as 300% in some cases, and this is detrimental to the long term Li cyclability since it give rise to "electrochemical pulverization" of the active material. This results in loss of electrical contact between the particles and current collector. This eventually leads to the electrode disintegration and capacity fading upon long-term cycling.

Four approaches have been used to combat this problem and they are as follows using first is the use of nanosize particles of the metals or oxides[26] or other compounds, which will enable them to absorb some of the volume changes because of the smaller number of atoms present in the nanograins and also the large surface area of the nanoparticles adds to it[26-27]. Second method is to incorporate one of the matrix elements, which are electrochemically active or inactive toward Li, such as Ca, Co, Al, Ti, and Ni. These help in volume changes and improve the electronic conductivity of the composite, and also act as catalysts for better Li cycling. Third approach is proper choice of the staring crystal structure and morphology. The fourth approach has been the choice of the proper voltage range for Li cycling. This is seen more prominent in the Sn oxides and the optimum voltage range is 0.005-0.8(or 1) V vs Li.

2.3.3.1 Binary Tin Oxides

Tin monoxide, SnO, adopts a tetragonal structure and is made up of SnO_6 octahedra. It is available as monocrystalline form but can also be prepared in micro- and nano- by various chemical methods. Uchiyama et al[28] reported a comparative Li cycling study of SnO of different morphologies with that of the commercial available SnO and reported to have obtained 760mAh/g for the initial capacities when compared to 525mAh/g for the commercially available one. However drastic fading was also reported to be seen in the sample.

Recently chowdaris group[29] has studied the nanocomposites $SnO(V_2O_3)_x$ and $SnO(VO)_{0.5}$ prepared from SnO and V_2O_3/VO by high energy ball milling (HEB) and examined the Li cycling properties by galvanostatic cycling and cyclic voltammetry. When cycled in the voltage range 0.005-0.8 V vs Li at a current of 60mA/g(0.12C) it showed a first charge-discharge capacity of 435mAh/g and stabilized around 380mAh/g.

Tin dioxide, SnO_2, adopts a tetragonal rutile structure. Guo et al[30] showed that a reversible and stable capacity of 700mAh/g can be obtained when the system is cycled in the range 0.005-1.0V up to 60 cycles. Zhu et al studied the Li cycling of SnO_2 nanoparticles with size ranging from 3 to 62 nm and obtained reversible capacities of 300-800 mAh/g, in the cycling range 0-1.0V at a current rate of $0.2mA/cm^2$. Other studies include SnO_2 with carbon nanotubes composites and they exhibit a range of 380 to 720 mAh/g. Zhao et al[31] prepared graphene nanosheet composites with two different mass ratios. They showed the second cycle capacity of 720mAh/g which stabilizes at 650mAh/g in the range 15-50cycles.

2.3.3.2 Ternary Tin Oxides

The Li cycling mechanism for ternary/quaternary oxides, M_xSnO_y, during the first discharge reaction with Li metal always involves the destruction of the crystal structure or amorphization of the lattice. This result in the formation of metal (M) or metal oxides (MO_y) and formation of nano-Sn-metal dispersed in amorphous Li_2O. This is followed by alloy formation, $Li_{4.4}Sn$.

The compounds M_2SnO_4 (M= Mg, Mn, Co, or Zn) adopt a spinel structure with Sn in tetrahedral coordination. Li cycling behavior of these oxides is in the range of 0.02-1.5V vs Li at low current rates. We were interested in the Zn_2SnO_4 (ZTO) for its properties and also wanted to pursue making new nanostructures. We were successful in getting some new unique structures which showed good performance and cyclability. A good review article was published by Baruah and Dutta[32] where they show different ways ZTO is made and its various applications. Then Zhe chen et al[33] showed new ZTO flower like nanostructure which were used for gas sensing applications.

Then there are oxides of the type $ASnO_3$ (A= Ca, Sr, Ba, Co, and Mg) which contains SnO_6 octahedra and adopts a pervoskite structure. Chowdari group have shown excellent cycling performance of $CaSnO_3$ with a reversible capacity of 380mAh/g stable up to 100 cycles in the voltage range 0.005-1.0V at 60mA/g.

2.3.3.3 Antimony Oxides and Mixed Oxides

Antimony has received attention, similar to Sn, due to its high specific capacity via alloying-dealloying reaction. But there have been problems of large volume variation which have caused problems. Binary oxides are Sb_2O_3, Sb_2O_4 and Sb_2O_5 of which Sb_2O_3 is the most stable. During the discharge cycle, Sb_2O_3 undergoes structure destruction and formation of the elemental Sb and Li_2O.

Chen[34] group studied the Li cycling of Sb_2O_3 in the range 0-2.0V at a current of 0.2mA cm^{-2} and they found a first charge capacity of 500mAh/g which slowly degraded to 300mAh/g after 10 cycles. Tarascon[35] group reported preliminary Li cycling properties of Sb_2O_3, Sb_2O_4 and Sb_2O_5 and found that the latter compound is electrochemically inactive. Bryngelsson et al[36] prepared Sb/Sb_2O_3 thin films on Ni-substrates by electrodeposition technique, and these exhibited a capacity of 660mAh/g stable for more than 50 cycles when they were cycled at a current rate of 0.1C in the range 0-1.5V.

Tarascon[35] studied the Li cycling of the compounds MSb_2O_6, M = Co, Ni, and Cu, which possess the trirutile structure. They showed that for M=Co and Ni, structure destruction occurs during the first discharge with the formation of Co or Ni metal and Sb particles at ~ 1.5V vs Li. The compounds with M=Co and Ni showed first-cycle reversible capacities of 400-450mAh/g when cycled in the range 0-3.0V at 0.05C.

2.4 Zinc Tin oxide

Zinc Tin oxide (ZTO) has been the focus of our research for its unique properties in the application of Lithium-ion battery. Zinc tin oxide has been considered as a promising candidate for transparent electrode, sensor, and photovoltaic devices. We have used high temperature calcination to prepare the material from Zinc hydroxystannate. Zhe chen[33] et al have prepared novel Zn_2SnO_4 hierarchical nanostructures. The 3-D nanostructures have been prepared using a one-step hydrothermal route at 180°C. The morphology of the final products was found to depend strongly on the concentrations of EDA and CTAB used. Some of the methods used to produce ZTO are as follows.

Different methods of Synthesis of ZTO	Studied by (authors)
Thermal Evaporation	Hanyuan chen et al.[37]
High-temperature calcination	Jie J et al.[38]
Sol-gel synthesis	Fu G et al.[39]
Hydrothermal reaction	Zhang et al.[40]
Ion-exchange reaction	Kovacheva et al.[41]

Table 1: Literature survey of different methods of synthesis for Zinc Tin oxide.

A.Rong et al[42] prepared spinel Zn_2SnO_4 particles with non uniform cubic shape via a hydrothermal process. They show that the conditions of reaction temperature and time are an important factor in the formation of the particles. The cube-shaped Zn_2SnO_4 particles with the spinel structure exhibit a large electrochemical capacity of 988 mAh/g and relatively good capacity retention as anode materials for Lithium-ion battery. They increase the concentration of NaOH steadily and that in turn gets sharper XRD peaks.

Hongliang Zhu et al[43] synthesized Zn_2SnO_4 Nanorods using hydrothermal synthesis, these were of the size of 2-4nm in diameter and around 20nm in length. They used hydrazine hydrate as an alkaline mineralizer instead of NaOH. Using the hydrothermal method they were able to bring down the ZTO diameters to around sub-5 nm range.

Xianghui Hou et al[44] synthesized Zn_2SnO_4 crystals by a solid state reaction using $Zn(NO_3)_2 \cdot 6H_2O$, $SnCl_4 \cdot 5H_2O$, and NaOH as the raw materials. In their XRD analysis they show Inverse spinel Zn_2SnO_4 with trace amounts or rather peak of SnO_2. They obtained a cubic like shape crystals with smooth boundaries and were in the size range of 100-500nm.

Wentao Song et al[45] prepared a layered Zn_2SnO_4/graphene nanohybrid anode which showed good performance in battery testing. A Zn_2SnO_4-nanocrystals/graphene-nanosheet nanohybrid has been prepared by a facile in situ hydrothermal route using $SnCl_4 \cdot 5H_2O$, $ZnCl_2$ and graphite oxide (GO) as the precursors and $N_2H_4 \cdot H_2O$ as the mineralizer and reducing agent. The nanocrystals formed are uniformly anchored on the graphene and help in the electrochemical activity.
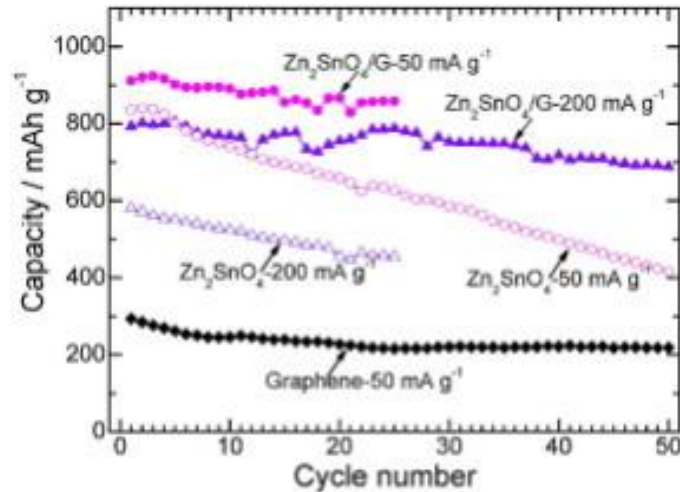
Figure 7: Cycling performance of Zn_2SnO_4/G and Zn_2SnO_4 charged at 50 and 200 mA g^{-1} and discharged at 50 mA g^{-1}, and bare graphene charged–discharged at 50 mA g^{-1} as shown[45].

X.J Zhu et al[46] synthesized Zn_2SnO_4 by hydrothermal process using NaOH as an alkaline mineralizer. In their synthesis they were able to synthesis Zn_2SnO_4 with trace amounts of ZnO and SnO_2 which were detected through XRD analysis. Jae-Wook Lee et al[47] tried synthesizing Zn_2SnO_4 by using supercritical water in a batch reactor. They used Zinc nitrate and tin chloride. NaOH was used to adjust the pH of the solution. The XRD results showed a combination of Zn_2SnO_4, ZnO and SnO_2.

Jingzhou Yin[48] et al have shown controlled growth of the $ZnSn(OH)_6$ which includes shapes such as cubes,cuboctahedrons,truncated octahedrons, and octahedrons using a solvothermal method in a methylcellulose ethanol/water solution. Adjusting the NaOH solution to the system they were able to observe shape evolution. Similarly we have been adjusting NaOH solution and were able to obtain cubes and spheres without adding the methylcellulose to the ethanol/water solution and then we were able to calcinated and through the CVD process obtain a layer of carbon on the cubes.

21

Chapter 3 Carbon Coated Cubic Mesostructure of Zn₂SnO₄@Sn@C for Reversible Lithium

Storage

3.1 Introduction

The performance of any device depends intimately on the properties of the materials of which it is formed and this holds for lithium batteries. We wanted to use transition metal oxides as electrode materials for next generation rechargeable lithium-ion batteries which have been widely studied. We wanted to improve these by nanoarchitecturing the electrodes to our specific needs. We have chosen the Zinc tin oxide system for use in the batteries. The main challenges that are seen in these batteries are low intrinsic electronic conductivity and severe volume changes during Li insertion/extraction processes, leading to poor cycling performance. We tried to overcome these problems by using carbon-coatings and using nanoarchitectured electrodes.

Zinc stannate (Zn_2SnO_4) also called Zinc tin oxide (ZTO) is acknowledged for having high electron mobility, high electrical conductivity and attractive optical properties that make it suitable for a lot of applications. Instead of breaking up the macro-material to nanostructures which uses more sophisticated equipment we use simple lab methods to make synthesis nanostructures thus making it more viable when viewed commercially.

There have been attempts to improve the performance through carbon usage. Sn-C composites have been created to improve the performance[49]. There are other papers that used similar approach where they nano-paint a layer of carbon on the nanostructure[50]. Carbon nanotubes (CNT) have also been used extensively to improve the electrode performance[51] as these have superior electrical conductivity and high activated surface area

and structural flexibility. We propose a new structure to which we have used the CVD method to nano-paint the microstructure, which is through CVD process. We show that anodes comprised of this structure and layering show good discharge rate capabilities and have good cycling performance. This can be understood with the following diagram.
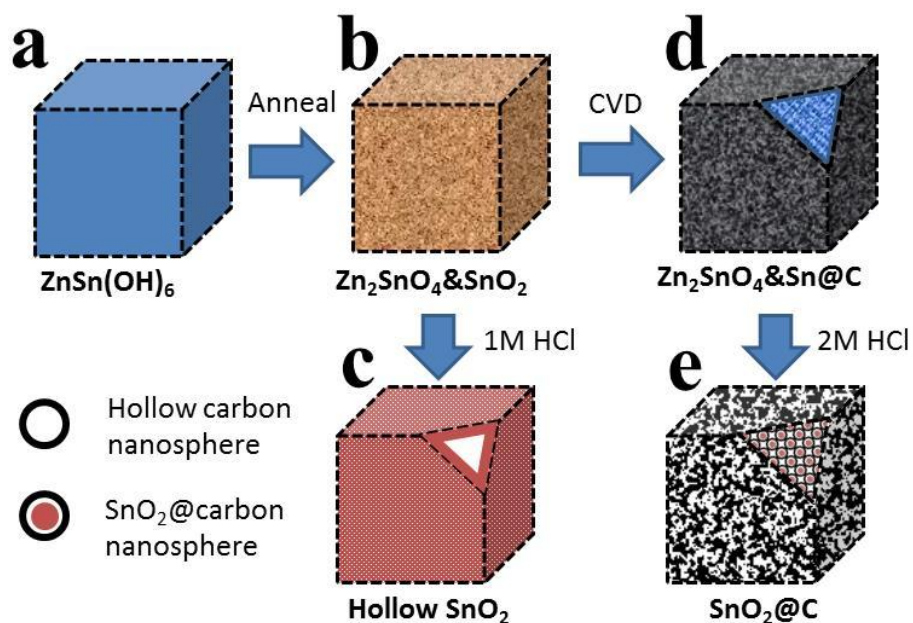
Figure 8: Schematic of preparation of a family of cubic mesostructures with different compositions: (a) $ZnSn(OH)_6$, (b)$Zn_2SnO_4\&SnO_2$, (c) hollow SnO_2 mesocubes prepared by etching $Zn_2SnO_4\&SnO_2$ mesocubes with 1M HCl, (d) porous $Zn2SnO4\&Sn@C$ mesocubes prepared by CVD Process,(e) porous mesocubes of SnO_2@carbon sphere aggregations obtained by etching $Zn_2SnO_4\&Sn@C$ mesocubes with dilute HCl.

Figure 1 illustrates the processes to prepare a family of mesocubes with different compositions. The precursors, $ZnSn(OH)_6$ mesocubes, were synthesized through a room temperature self- templating co-precipitation method. (Figure 1a) The Zn_2SnO_4&SnO_2 mesocubes were prepared by calcinating $ZnSn(OH)_6$ mesocubes at $800^O C$ for 1h. (Figure 1b) SnO_2 mesocubes were prepared by removing Zn^{2+} from Zn_2SnO_4&SnO_2, which was prepared at $650^O C$ for 6h, using 1M HCl solution. (Figure 1c) The Zn_2SnO_4&Sn@C mesocubes were prepared through a CVD treatment of Zn_2SnO_4&SnO_2, which was prepared at $800^O C$ for 1h, with flow of acetylene/argon at $650^O C$ for 1h. (Figure 1d) Porous mesocubes aggregated by SnO_2@carbon Nanospheres can be prepared from Zn_2SnO_4&Sn@C by washing with 2M HCl solution for 2days. (Figure 1e)

3.2 Experimental

3.2.1 Preparation and characterization

a. ZnSn(OH)$_6$ mesocubes: The ZnSn(OH)$_6$ precursor was synthesized through a room-temperature self-templating co-precipitation method. In a typical synthesis, 50ml of ethanol solution containing SnCl$_4$ (0.025M) and ZnCl$_2$ (0.05M) was prepared. Then 50ml of aqueous solution of NaOH (0.32M) was added drop wise into the ethanol solution in 5 minutes. The mixture was stirred for one hour and the reaction was lasted for another 23h without stirring. The resulting white precipitate was collected by centrifugation, washed with ethanol and deionized water for several times to remove residual ions in the products. The ZnSn(OH)$_6$ precursor was then dried in air at 100°C for 24hr before characterization.

b. Zn2SnO4&SnO$_2$ mesocubes: The Zn$_2$SnO$_4$&SnO$_2$ mesocubes were prepared from ZnSn(OH)$_6$ precursor through a calcination process. To prepare Zn$_2$SnO$_4$&SnO$_2$ mesocubes with small grain size which are more vulnerable to acid etching, the ZnSn(OH)$_6$ powder was placed into a ceramic crucible and heated at 650°C for 6h, with ramping rate of 1^{O}C/min in air. To prepare porous Zn$_2$SnO$_4$&SnO$_2$ mesocubes with larger grain size which favors the transportation of chemical vapor inside the mesocubes, the ZnSn(OH)$_6$ powder was placed into a ceramic crucible and heated in a quartz tube furnace at 800°C for 1h, with ramping rate of 20°C/min under Ar flow.

c. Hollow SnO2 mesocubes: SnO$_2$ mesocubes were prepared by an acid etching process. The precursor of SnO$_2$ mesocubes was prepared by calcinating ZnSn(OH)$_6$ in air at

650^OC for 6h, with ramping rate of 1^OC/min. 50mg of Zn_2SnO_4&SnO_2 mesocubes prepared at 650^OC were dispersed in 40ml of 1.0M HCl for 24h at room temperature under stirring. The white product was collected by centrifugation, washed with deionized water for several times until the solution became neutral and then washed with ethanol, dried at 60°C.

  d. Zn_2SnO_4&Sn@Carbon mesocubes: The Zn_2SnO_4&Sn@Carbon mesocubes were prepared through a CVD process. In a typical synthesis, the porous Zn_2SnO_4&SnO_2 mesocubes prepared at 800^OC were placed into a ceramic crucible and heated to 650^OC in a quartz tube furnace with ramping rate of 20^OC/min under Ar flow. The CVD process was carried out at 650^OC for 1h with a flow of 100sccm of mixture gas (10% acetylene in argon). The tube furnace was cooled down with pure argon flow after 1h of CVD process.

  e. Porous $SnO2$@C mesocubes: SnO_2@C mesocubes were prepared from Zn_2SnO_4&Sn@Carbon mesocubes by acid etching process. In a typical procedure, 25mg of $Zn2SnO4$&Sn@Carbon mesocubes was dispersed into 20ml of 2M HCL for 2 days, the acid etched product in black color was collected by centrifugation, washed with deionized water for several times until the solution became neutral and then washed with ethanol, dried at 60°C.

3.2.2 Electrochemical measurements

Electrochemical Measurements: Homogeneous slurry was prepared by mixing 80wt% of the as prepared active materials, 10wt% of conductivity enhancer (Super-P carbon black, Timcal), and 10wt% of polyvinylidene fluoride (PVDF) binder in N-methylpyrrolidone (NMP). The slurry was then applied to copper discs as current collectors and dried in a vacuum oven at 80°C for 24h. Coin-type cells were assembled in an argon-filled glove box using the coated copper disc as the working electrode, metallic lithium foil as the counter electrode, 1 M solution of LiPF6 in a mixture of ethylene carbonate (EC) and diethyl carbonate (DEC) (1:1, v/v) as the electrolyte, and PP/PE/PP trilayer membrane (Celgard 2320) as the separator. The electrochemical cells were charged and discharged galvanostatically at room temperature in the voltage window of 0.005V-3V on a MTI BST8-WA battery tester.
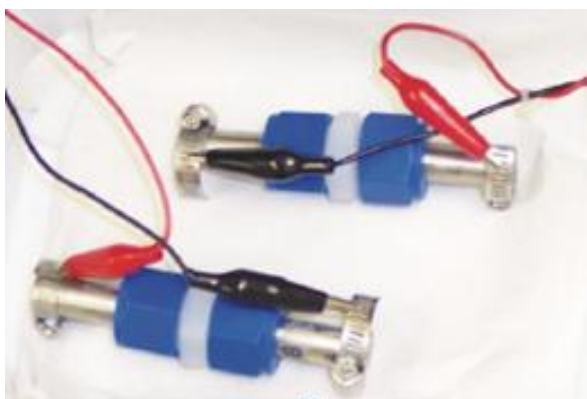
Figure 9: Battery cells being analyzed by the MTI instrument.

3.3 Results

3.3.1 XRD

X-ray powder diffraction (XRD) pattern was recorded using a Regaku X-ray diffractometer equipped with graphite monochromatized Cu-Kα radiation with a scanning rate of 4°C min^{-1}. From the X-ray analysis using Jade we were able to see that the formed microstructure cubes are $ZnSn(OH)_6$. All the diffraction peaks can be assigned to $ZnSn(OH)_6$ according to the standard JCPDS no. 20-1455, the following figure shows the XRD spectra.
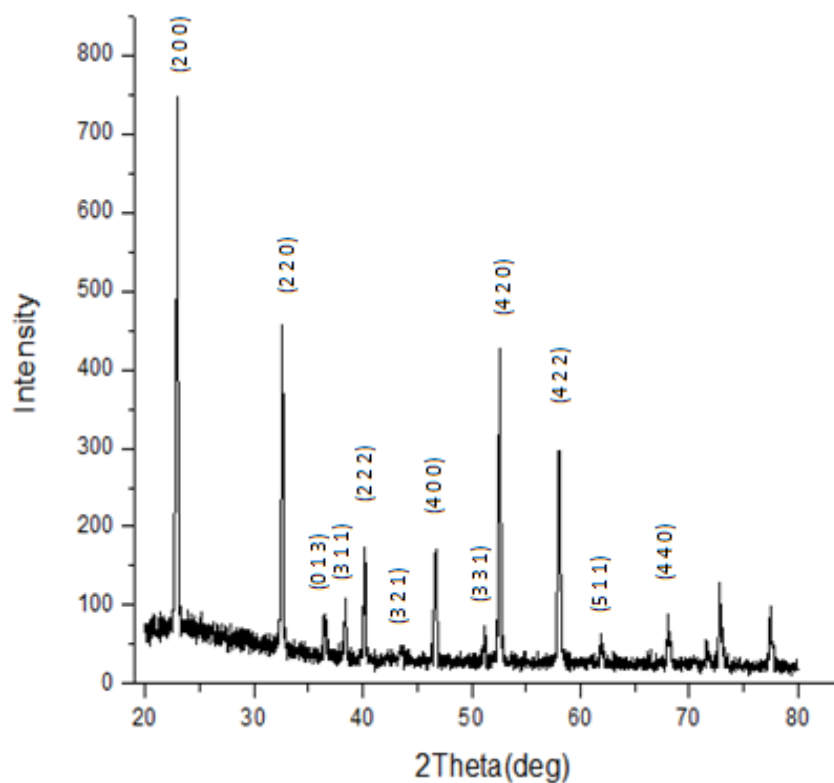
Figure 10: XRD pattern of $ZnSn(OH)_6$ prepared by the facile method

The obtained $ZnSn(OH)_6$ on calcination gave the mixed phase of Zn_2SnO_4/SnO_2 , this could be seen from the XRD results for the calcinated sample. All the diffraction peaks can be assigned to Zn_2SnO_4 to the JCPDS no.   and SnO_2 according to the standard JCPDS no. 74-2184, the following figure shows the XRD spectra.
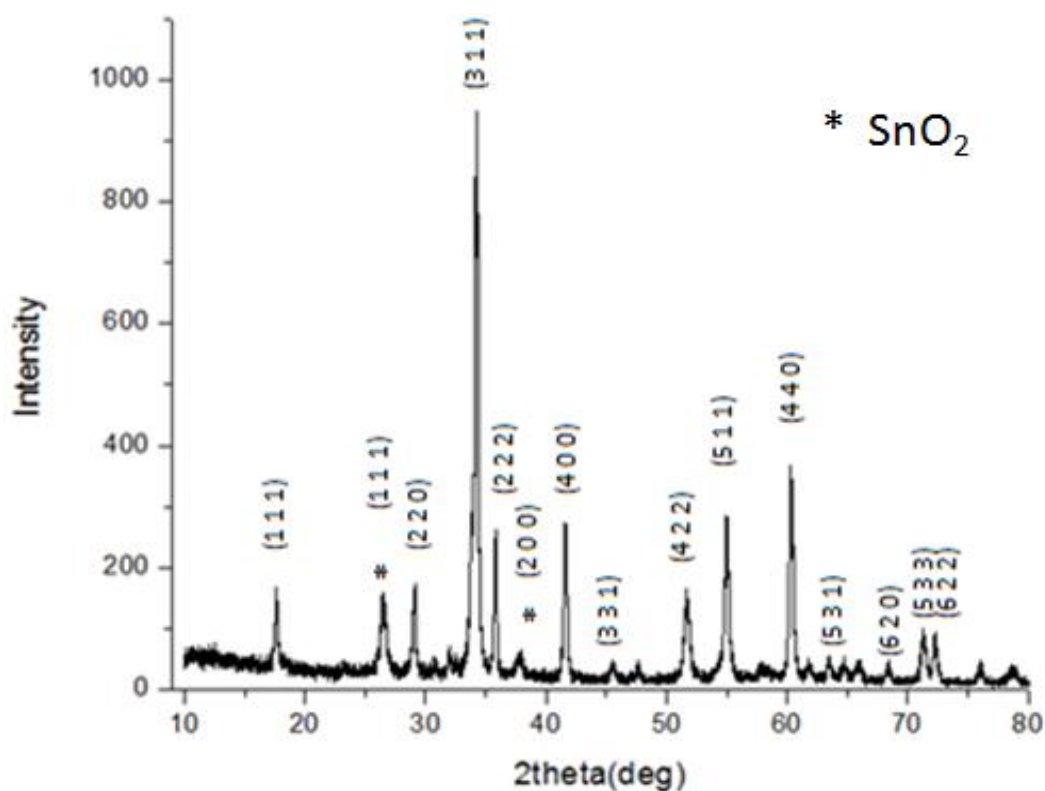
Figure 11: XRD pattern of Zn_2SnO_4/SnO_2 after calcination of Zinc hydroxystannate

From the analysis of the XRD by the Jade software we could see that the composition of the as obtained products are not exactly phase pure Zn_2SnO_4 rather it has also has peaks showing SnO_2. Specifically speaking we were able to see peaks of SnO_2 at 26.3 2theta (degrees) and at 38 degrees which are clear. From the existing literature we could see that the process of calciantion follows the following reaction and forms a Zn_2SnO_4/SnO_2 composite.

$$2ZnSn(OH)_6 \rightarrow Zn_2SnO_4 + SnO_2 + 6H_2O \text{ at } 800°C$$
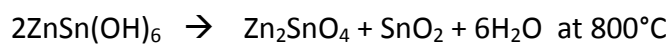
We further use the CVD process to grow a layer of carbon the microcubes. The layer of carbon is around few nanometers and this can be clearly seen in the TEM image. We also used XRD to check the changes that have been caused in the phase of the system. All the diffraction peaks can be assigned to Zn_2SnO_4 to the standard JCPDS no. 74-2184. The XRD for after 1 hr CVD process of the Zn_2SnO_4 /SnO_2 is as follows.
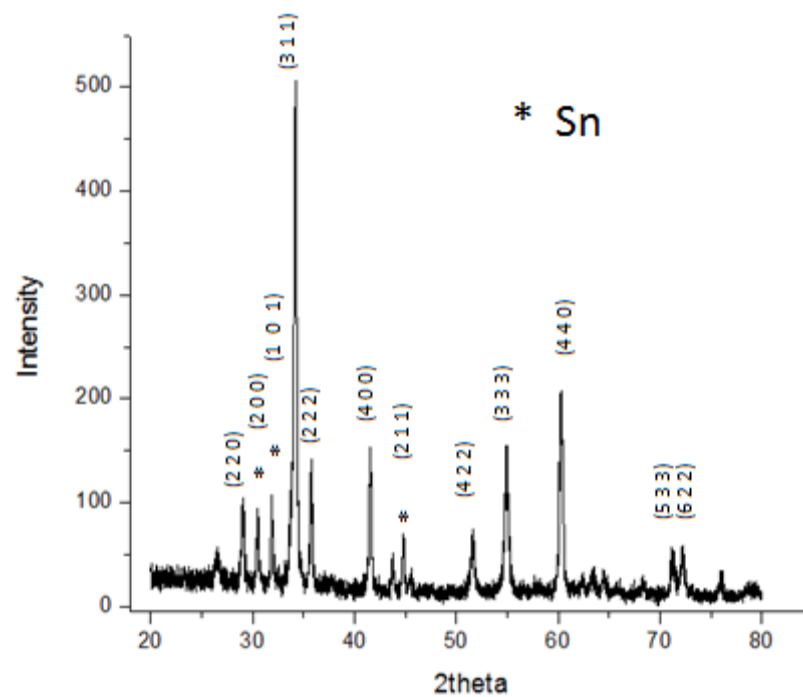
Figure 12: XRD pattern of Zn_2SnO_4/Sn@C Mesocube after the 1hr CVD process.

From the above XRD we could see sharp peaks of the element 'Sn' after 30 degrees. Trace amount of SnO_2 is still observed due to incomplete reduction.

We further increase the CVD time to 3hr for the Zn_2SnO_4/SnO_2 cubes and we find the following XRD of the obtained material. Here we can clearly see from the previous XRD of 1hr that the amount of metal 'Sn' has increased.
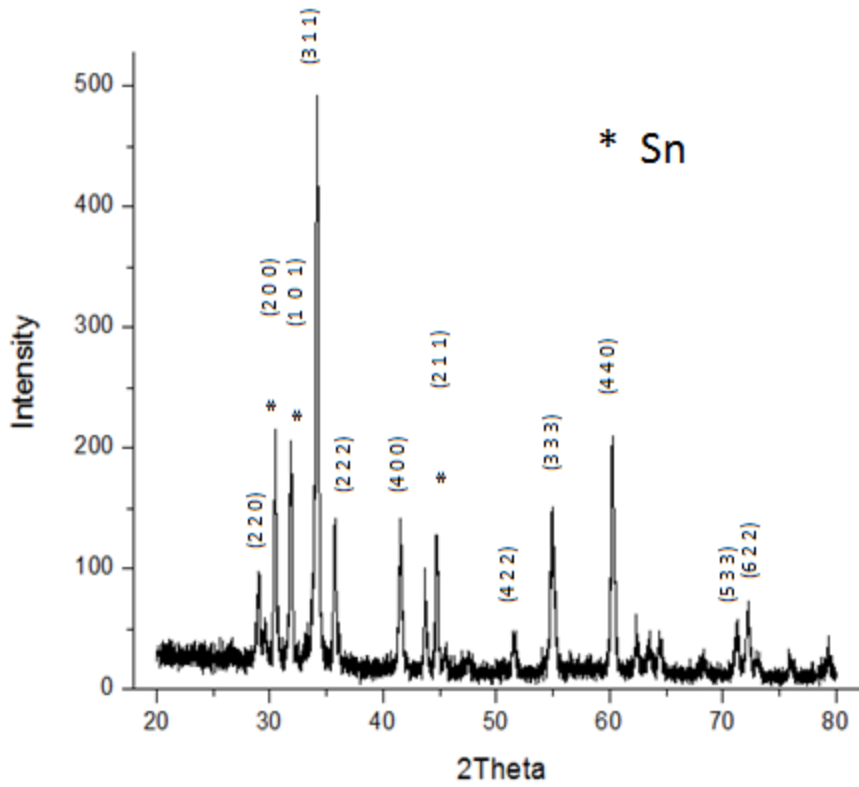
Figure 13: XRD pattern after 3 hr CVD process.
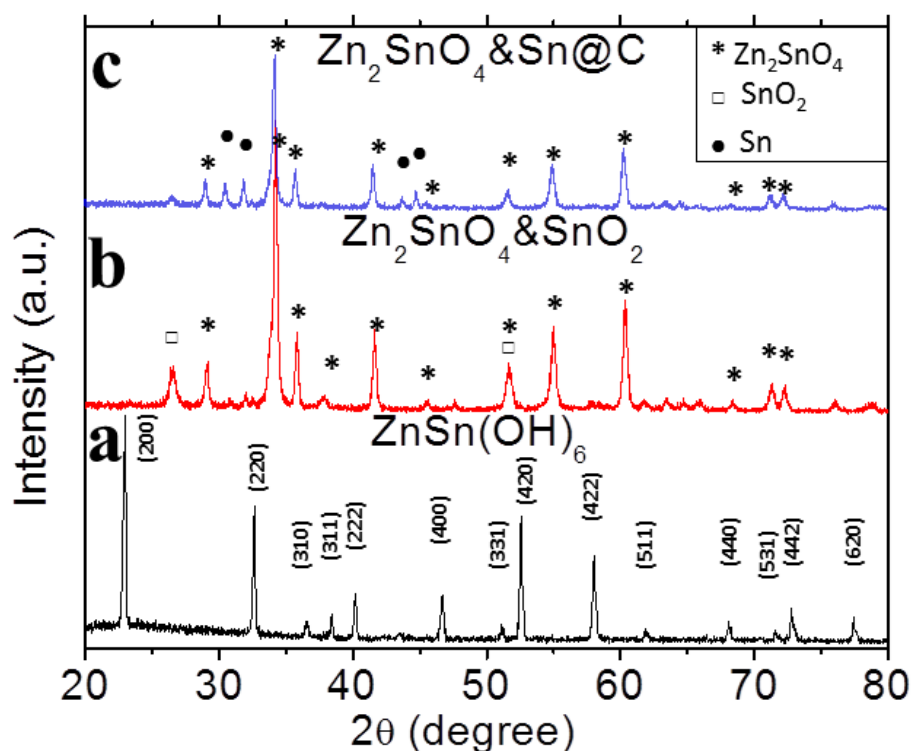
Figure 14: XRD patterns of samples (a) ZnSn(OH)$_6$ precursor,(b) Zn$_2$SnO$_4$&SnO$_2$ obtained by calcination at 800°C, and Zn$_2$SnO$_4$&Sn@C obtained by CVD for 1h, respectively.

The XRD patterns of precursor, calcinated sample and CVD sample are shown in Figure 14. The XRD pattern of precursor prepared through room-temperature self-templating co- precipitation method can be assigned to primitive cubic ZnSn(OH)$_6$ (JCPDS card no. 20-1455), as shown in Figure 14a. No other peak was observed, indicating the purity of as-prepared materials. The XRD pattern of sample prepared by calcinating precursor at 800°C was shown in Figure 2b, which can be assigned to Zn$_2$SnO$_4$ with cubic crystal structure (JCPDS card no. 24-1470) and tetragonal rutile SnO$_2$ (JCPDS card no. 41-1445). After the chemical-vapor deposition (CVD) process in

acetylene/argon, the composition of the products changed to the mixture of Zn_2SnO_4 with cubic crystal structure (JCPDS card no. 24-1470) and tetragonal tin (JCPDS card no. 01-0926). The distinguishable peak at around $2\theta=26°$ for SnO_2 in Figure 14b disappeared in Figure 14b, indicating the successful reduction of SnO_2 to Sn by acetylene through CVD process, which was also reported in other works.[52,53,54,55.]

3.3.2 FESEM and TEM
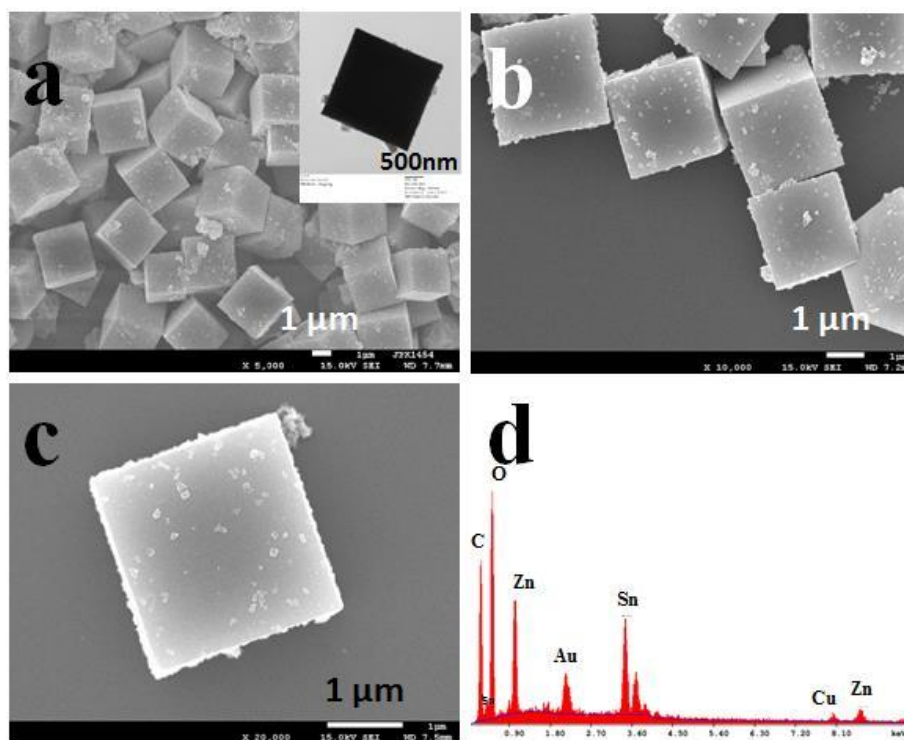
Figure 15: ZnSn(OH)6 mesocubes: (a-c) FESEM images and (d) EDS of cubic ZnSn(OH)6 precursor obtained at room temperature with 0.32M NaOH. Inset of (a) is the TEM image of cubic ZnSn(OH)6 precursor

The morphology of as-prepared precursor, ZnSn(OH)$_6$ mesocubes, was revealed by the FESEM images at different magnifications in Figure 15a-c. The ZnSn(OH)$_6$ in cube-like structure are uniform with sizes about two micrometers, as shown in the low-magnification FESEM image(figure 15a). The magnified FESEM image shows the regular cubic like structure of as prepared ZnSn(OH)$_6$ precursor, including the very flat surfaces and sharp edges(Figure

15b-c). The typical cubic structure and the solid nature of the mesocubes were revealed by the TEM image (inset of figure 15a).As compared to the all the products which were prepared under high temperature, the $ZnSn(OH)_6$ is more condensed and has a lower porosity, as proved by the smooth surface of the cube in FESEM and the very dark area of the cube shown in TEM. The EDS of $ZnSn(OH)_6$ was shown in Figure 15d, the atomic ratio of Zn:Sn is 1:1, which is in accordance with the XRD pattern in Figure 14a.
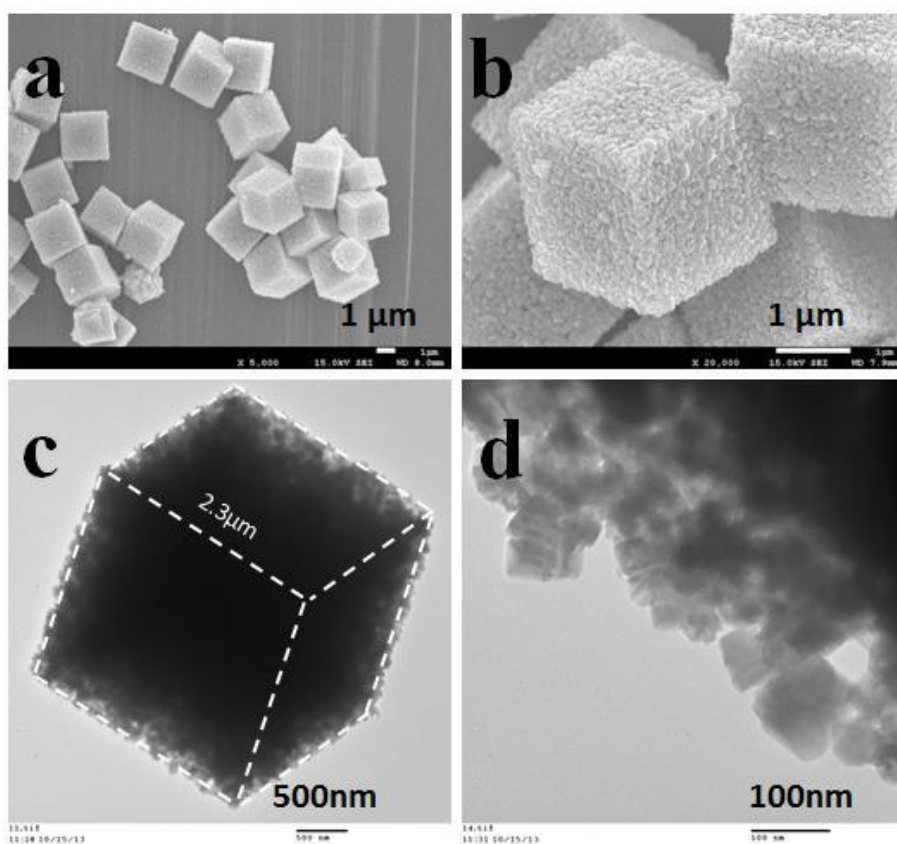
Figure 16. Zn_2SnO_4&SnO_2 mesocubes: (a, b) FESEM and (c, d) TEM images of the Zn_2SnO_4&SnO_2 mesocubes obtained by calcinating cubic $ZnSn(OH)_6$ precursor at $800^{o}C$ in argon

The porous $Zn_2SnO_4\&SnO_2$ mesocubes were obtained by calcinating close-compacted $ZnSn(OH)_6$ precursor at 800 C for 1h, and the morphology of the $Zn_2SnO_4\&SnO_2$ was revealed by FESEM and TEM, as shown in Figure 16.The uniform and the distributed mesocubes were observed in Figure 16, the cubic structure was preserved after the high temperature annealing process without change in size or shape. More details were revealed in magnified FESEM image (Figure 16b). The surface of the $Zn_2SnO_4\&SnO_2$ mesocubes became coarser than the surface of $ZnSn(OH)_6$ mesocubes, and the subunits which aggregate to form the mesocubes can be observed, due to the increase of grain size under high temperature calcination process.[56] The TEM image for a typical $Zn_2SnO_4\&SnO_2$ mesocube was shown in Figure 16c, the course edges and the nano-sized subunits can be observed, and the size of this typical mesocubes was 2.3 μm. The magnified TEM image (Figure 16d) shows the subunits in nanoscale. All the nanoparticles are less than 100nm in size, the structure became porous as compared to the closely compact $ZnSn(OH)_6$ cubes and then there are some void space among those nanoparticles aggregations. The $Zn_2SnO_4\&SnO_2$ materials prepared at a high temperature of 800^OC with porous property were used to prepare $Zn_2SnO_4\&Sn@C$ materials through CVD process. The porous structure allows the diffusion of chemical vapor inside the cubes in micro scale and facilitates the vapor deposition process throughout the mesocubes. The porosity of the structure of $Zn_2SnO_4\&SnO_2$ can also be proved by the uniform coating of carbon of $Zn_2SnO_4\&Sn@C$ materials. The EDS result of as prepared $Zn_2SnO_4\&SnO_2$ was shown in Figure S1a, with molar ratio of Zn: Sn of 1:1. The atomic ratio of O (46.55 At %) was decreased compared to the atomic ratio of O in $ZnSn(OH)_6$ (77.26 At %) due to removal of the hydroxyl water during the heating

process and the conversion of $ZnSn(OH)_6$ to Zn_2SnO_4.[56,57,58,59] The reaction can be ascribed as following equation, which is also proved in the XRD pattern in Figure 14b:[59]

$$2ZnSn(OH)_6 \rightarrow Zn_2SnO_4 + SnO_2 + 6H_2O$$
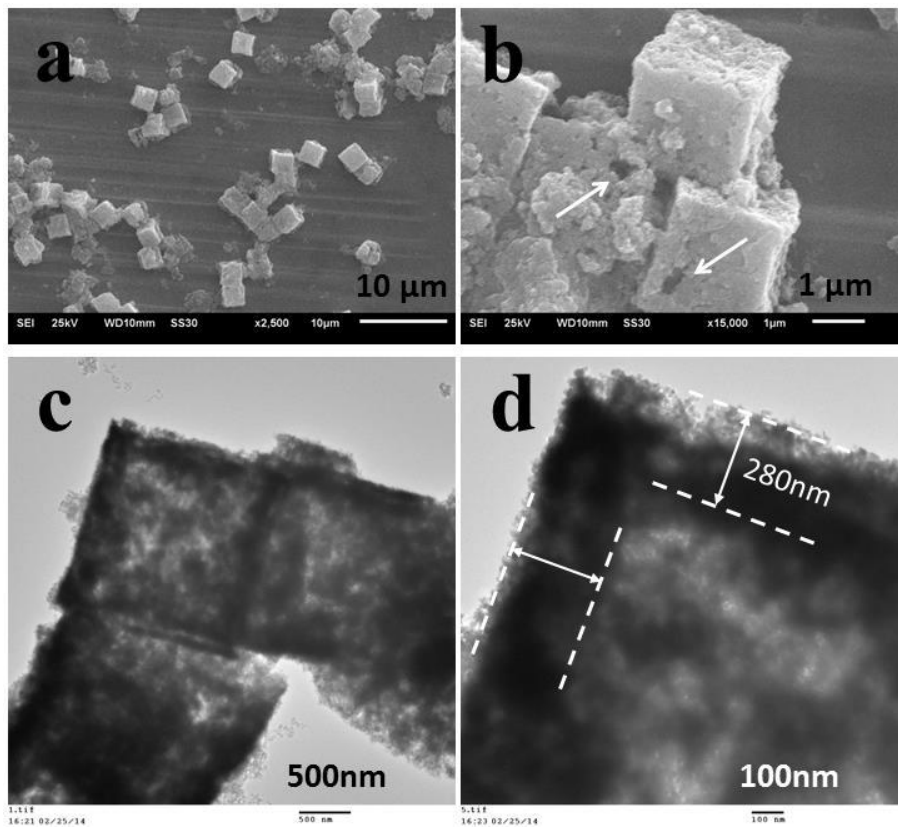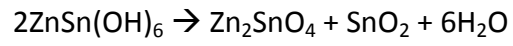
Figure 17: Hollow SnO_2 mesocubes: (a,b) SEM images and (c,d) TEM images of hollow SnO_2 mesocubes obtained by etching Zn_2SnO_4&SnO_2 mesocubes prepared at 650 C with 1M HCl for 1 day.

The hollow SnO_2 mesocubes were synthesized by etching Zn_2SnO_4&SnO_2 mesocubes, which were prepared at 650°C with 1M HCl for 1 day, with 1M HCl solution for 1day under stirring. And the morphology of as-prepared hollow SnO_2 mesocubes is revealed by SEM and TEM, as shown in Figure 17. The preservation of the cubic structure was demonstrated by the low- magnification SEM in Figure 17a. Due to the acid-etching effect, the Zn^{2+} can be removed by the dilute hydrochloride acid. Thus, porous hollow SnO_2 cubes formed after the acid-etching process.The typical cubic structure was shown in Figure 17b, the broken surface was pointed out by the white arrow. Due to the dissolvation of part of the solid composites, the size of cubes decreased a little bit from 2.2 micrometer. Besides, the surface of the cube was depressed and was no longer flat. This was possible due to that the void core was generated by the acid-etching process; the void core cannot support the outside surface as a solid core did. The hollow cubes were also demonstrated by the TEM image in Figure 17c; the void space created was cubic, around 1.1 micrometers in length. The corner of a typical etched hollow cube was shown in magnified TEM image, the thickness of the shell was measured to be 280nm, as shown in Figure 17d. The formation of hollow cubes, rather than the uniform porous cubes might be ascribed as following: During the heating process to prepare ZTO&SnO2 from $ZnSn(OH)_6$, the heat was transferred from the surface to the core part of the cube. Thus, the ZTO&SnO2 formed on the surface was earlier than the core part, and the larger grain size will be obtained on the surface due to the more sufficient heat received. Both of the factors make it harder to etch the shell than the core part. Also, it is suggested that the formation of hollow cubes through acid etching process might due to the loose and even porous matter at the core part of the materials in the work of Ma G. et al.[60] The removal

of Zn2+ is proved by the EDS in Figure S1b, compared to the EDS of Zn2SnO4&SnO2 in Figure S1a, the intensity of Zn peak decreased and the intensity of Sn increased. The peak of Zn is not distinguishable, which indicates most of the Zn^{2+} was removed by HCl solution.
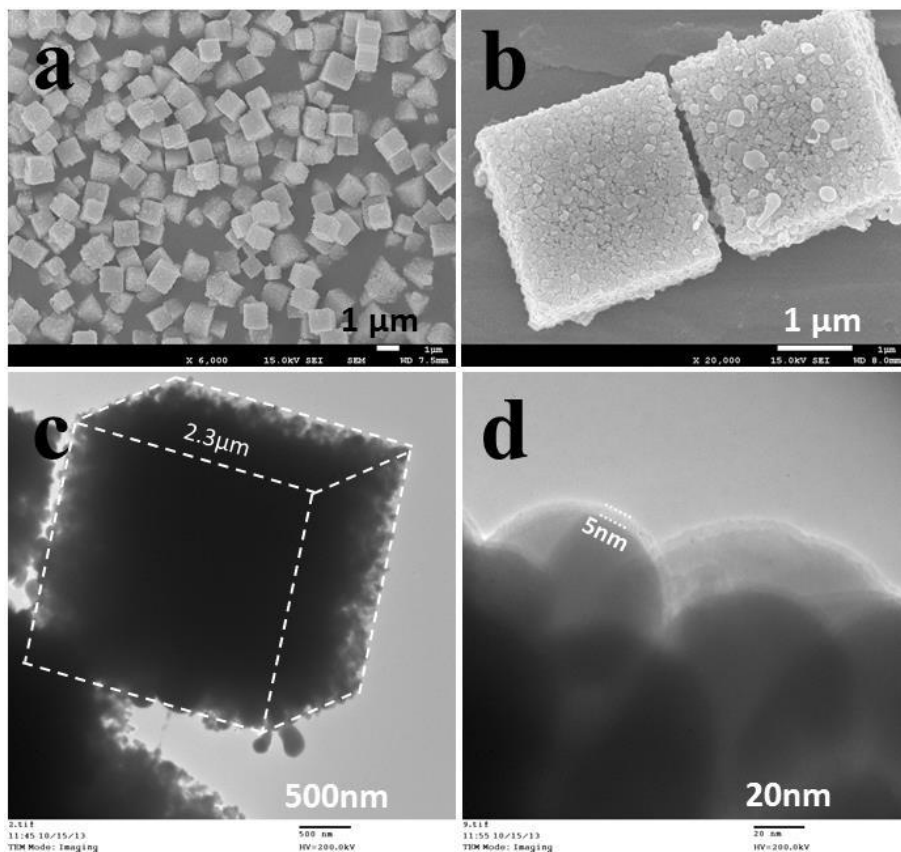
Figure 18: Zn_2SnO_4&Sn@C mesocubes: (a,b) FESEM and (c,d) TEM images of Zn_2SnO_4&Sn@C mesocubes obtained through CVD treatment of Zn_2SnO_4&SnO_2 mesocubes prepared at 800 C for 1hr.

3.3.3 EDS Elemental Mapping
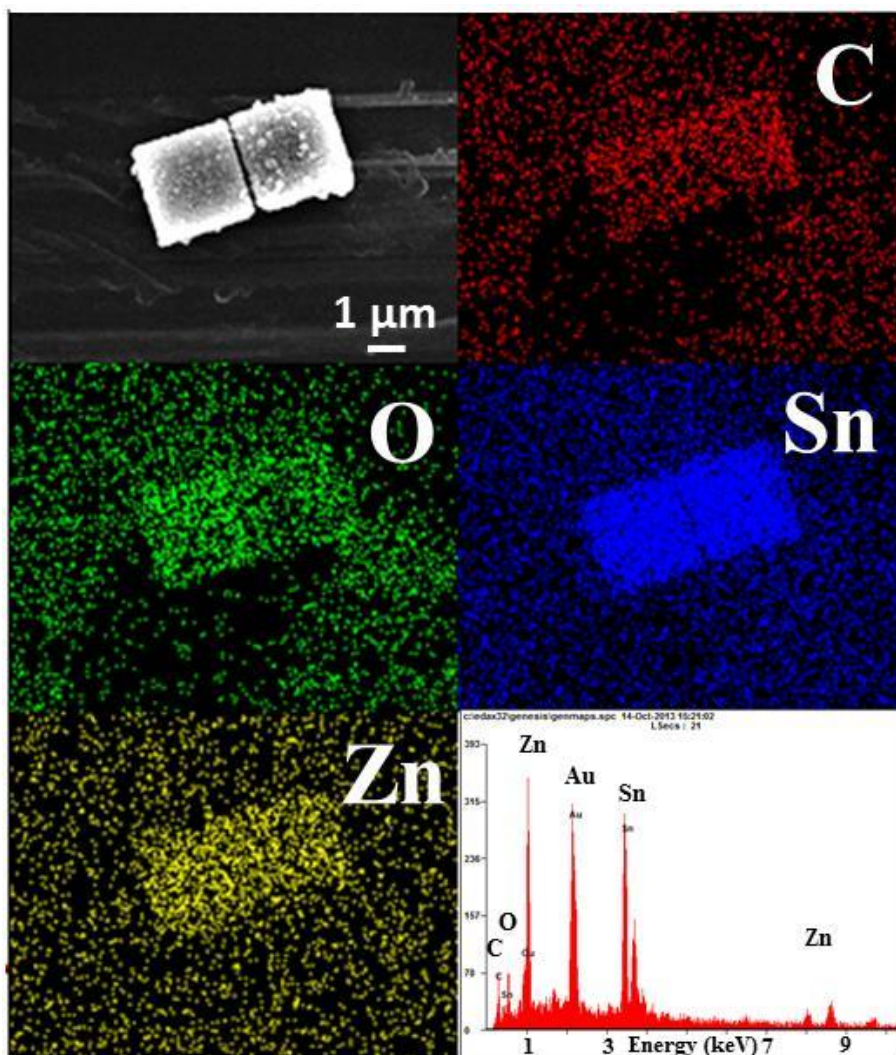
Figure 19: EDS elemental mapping of confined cubic mesostructure of $Zn_2SnO_4\&Sn@C$ obtained after 1hr CVD treatment of $Zn_2SnO_4\&SnO_2$ mesocubes.

Zn2SnO4&Sn@C mesocubes were prepared through 1h CVD process from Zn2SnO4&SnO2, which was prepared at 800oC. The existence of Sn was proved by XRD in

Figure 14c, which can be attributed to the reduction of SnO2 to Sn by acetylene gas. The morphology of the Zn_2SnO_4&Sn@C mesocubes was revealed by FESEM and TEM images in Figure 18.The uniform cubic structure was preserved after the CVD process, as shown in figure 18a. Two typical Zn_2SnO_4&Sn@C mesocubes are shown in magnified FESEM images in Figure 18b.The surface is smoother compared to the surface of Zn_2SnO_4&SnO_2 mesocubes due to the carbon coating formed during the CVD process. One broken carbon sphere can be observed on the surface of Zn2SnO4&Sn@C mesocubes, which also demonstrate the deposition of carbon on the cube. The TEM image for a typical Zn2SnO4&Sn@C mesocube was shown in Figure 18c. The size of Zn2SnO4&Sn@C mesocube is 2.3 μm, which is the same as the size of Zn2SnO4&SnO2 mesocubes. The Zn2SnO4&Sn@C mesocubes are aggregated by nanosize subunits, the details of the subunits are shown in Figure 18d. The nanoparticles which aggregate to form Zn2SnO4&Sn@C mesocubes are about 25nm in size, and are coated with a layer of carbon. The carbon uniformly covered all the nanoparticles and had a thickness of ~5nm. The EDS result and the elemental mapping of Zn2SnO4&Sn@C mesocubes were shown in Figure 19. The uniform distribution of all the elements, including C, O, Sn and Zn, on mesocubes was revealed by color of red, green, blue and yellow, respectively. The uniform distribution of carbon indicates that the carbon formed throughout the whole cubes, not just on the surface of it, which was further proved by the acid-etched products, SnO2@C cubes in Figure 20. It demonstrates that the Zn2SnO4&SnO2 materials which used as precursor in CVD process were porous, because the mesocubes are permeable to the chemical vapor and allow the carbon deposition at the core part of mesocubes. The atomic ratio of carbon is about 30%, as shown in EDS spectrum.
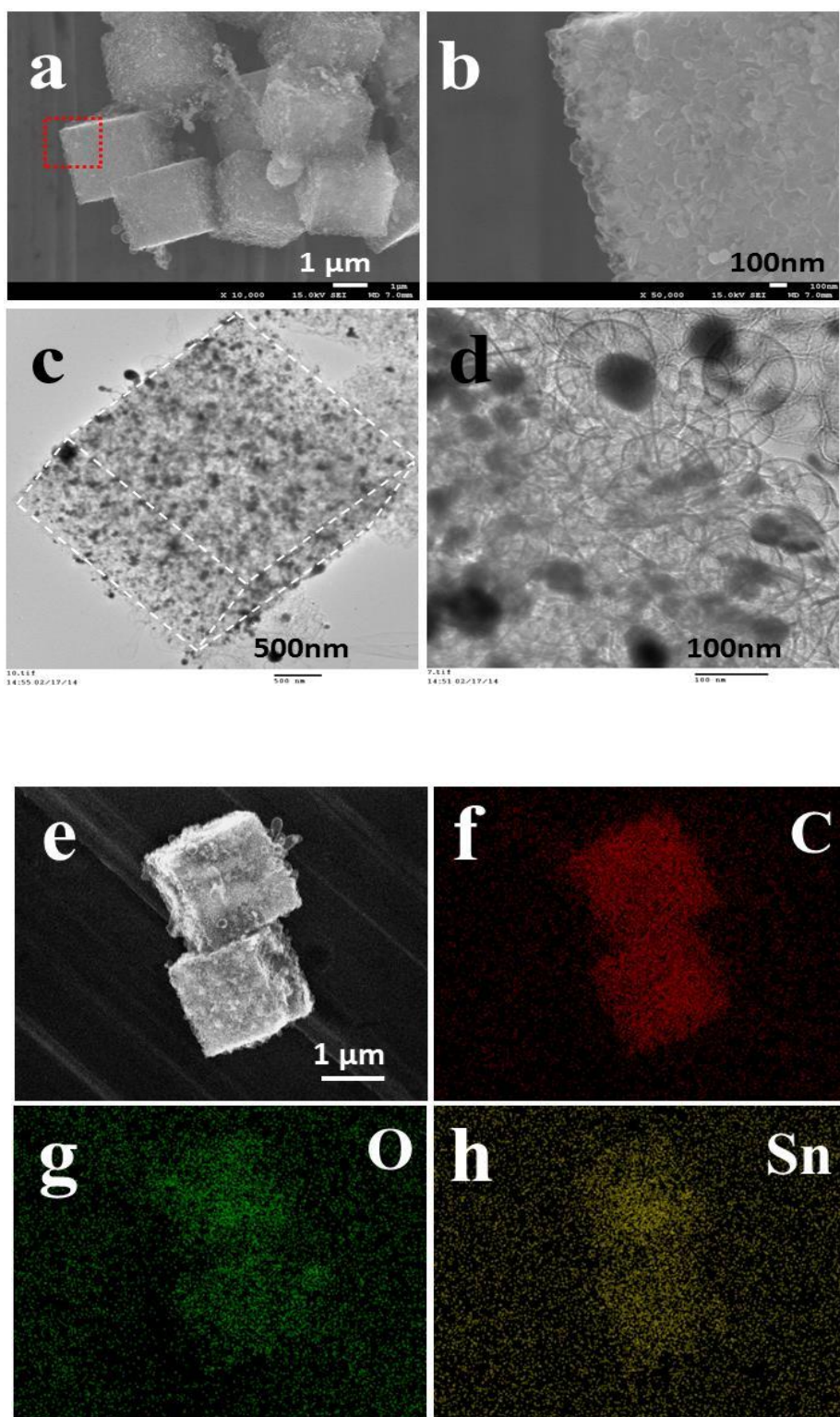
Figure 20. Porous SnO$_2$@C mesocubes: (a, b) SEM images and (c, d) TEM images (e-h) EDS elemental mapping of porous mesocubes of SnO$_2$@carbon sphere aggregations obtained by etching Zn$_2$SnO$_4$&Sn@C mesocubes with dilute HCl.

42

The mesocubes of SnO2@C nanosphere aggregations was obtained by etching Zn2SnO4&Sn@C mesocubes with dilute HCl solution. The uniform cubic structure with size about 2μm can be preserved after the acid etching step, as shown in the low magnification FESEM image (Figure 20a). The magnified FESEM shows more details about the nanosphere subunits at the corner of mesocubes (in the area marked by red dash) in Figure 20b. As compared to its precursor, Zn2SnO4&Sn@C mesocubes, SnO2@C mesocubes have coarse surfaces, which is due to the removal of Zn2SnO4 and Sn. The typical porous mesocube aggregated by hollow nanospheres was revealed by TEM images in Figure 20c. As compared to all the solid mesocubes before acid etching step, such as ZnSn(OH)6, Zn2SnO4&SnO2, Zn2SnO4&Sn@C, the acid- treated SnO_2@C mesocubes are highly porous and some hollow carbon spheres can be observed, which can be attributed to the removal Zn2SnO4 and Sn. A magnified TEM image in Figure 20d shows the details about the SnO2@C nanosphere subunits. The mesocubes were aggregated by SnO2@C nanospheres in size of <100 nm and small amount of hollow nanospheres can be observed on outside surface of the mesocube. The EDS result in Figure S1c shows that the carbon is the dominant composition with atomic ratio of 90.26%, while small amount (3.72 at%) of Sn element and O(6.03 at%) exist in the mesocubes. The EDS mapping of SnO_2@C mesocubes in Figure 20(e-h) demonstrates the uniformity of carbon, oxygen and tin on the mesocubes by red, green and yellow colors, respectively. Also, the mapping of carbon element, combined with the TEM images, proves the uniformly coating of carbon on all the nanosized subunits of mesocubes, not just on the surface of mesocubes. The removal of Zn and Sn was studies through time-dependent experiment. The EDS results of samples treated with 2M HCl were shown in figure 20.The removal of both Zn and Sn was demonstrated by the lasting increased content from 1h to 4h.With reaction increase from 1h to 4h, the contents of both Zn and Sn decreased from

20% to 3% after the acid treatment. Similar to the dissolvation of $ZnSnO_3$ reported,[61,62] the dissolvation of Zn_2SnO_4 might be ascribed by following equations:

$$Zn_2SnO_4 + 4H^+ \rightarrow 2Zn^{2+} + H_4SnO_4$$

$$H_4SnO_4 + 6HCl \rightarrow H_2[SnCl_6] + 4H_2O$$
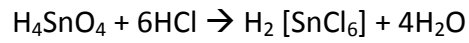
Even though H_4SnO_4 can be considered as the hydrous form of SnO2, which is hard to dissolve in water, it is not stable and can react with hydrochloride acid. Thus both Zn and Sn elements were removed by HCl solution.

3.3.4 Battery testing

We used the Zn_2SnO_4/SnO_2 in the battery as an anode material and where able to plot charge-discharge curves for it and also the capacity versus number of cycles plot.
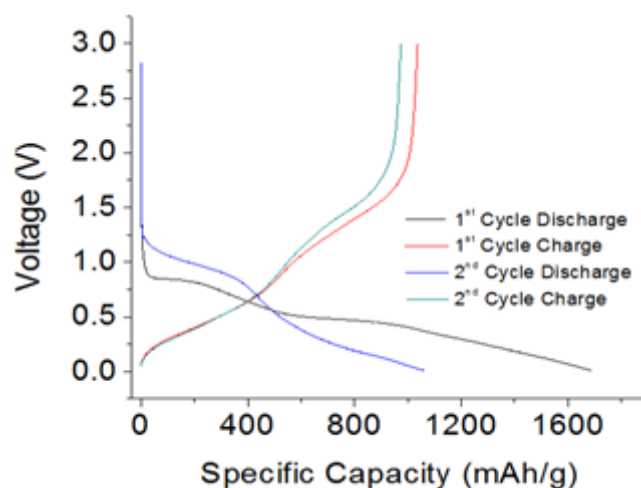
Figure 21: Discharge-charge curves for the Zn_2SnO_4/SnO_2 electrode.

As you can see from the plot the first three charge and discharge cycles for the battery has been drawn. Similarly we can plot capacity versus number of cycles as follows.
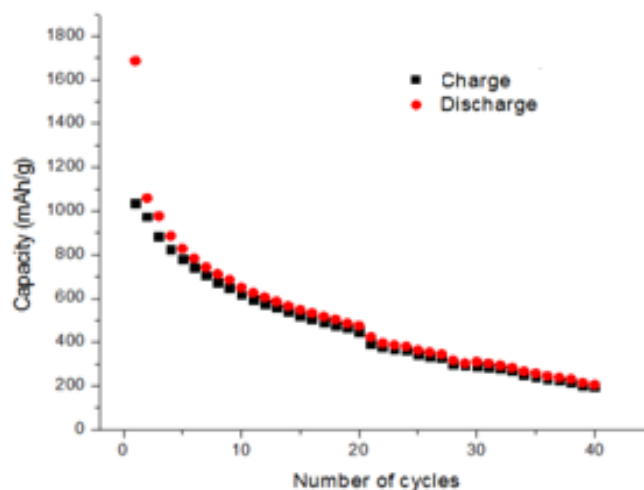
Figure 22: Cyclic life of the electrodes of the as-prepared Zn_2SnO_4/SnO_2.

We then plot the same way for Zn_2SnO_4/SnO_2 after the CVD process i.e. for the Zn_2SnO_4/SnO_2 which has a layer of carbon on it. And as above we have the first three charge and discharge cycles and the capacity versus number of cycles plot shown below.
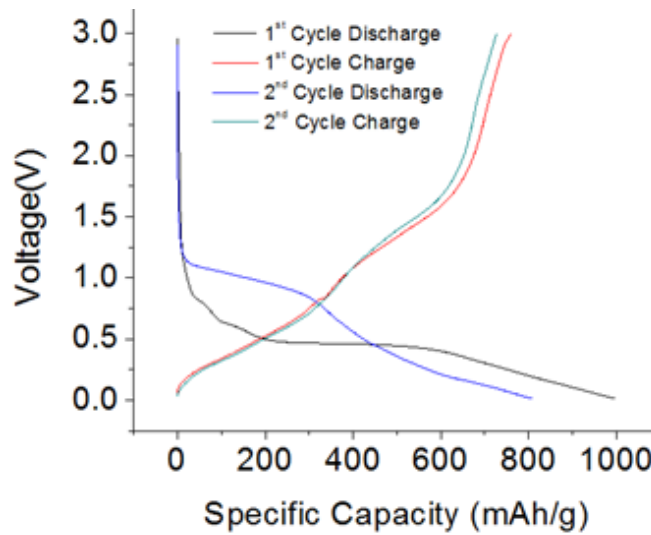
Figure 23: Discharge-charge curves for the Zn_2SnO_4/SnO_2 electrode after carbon coating.

Then similarly the capacity versus number of cycles plot for Zn_2SnO_4/SnO_2 after the CVD process.
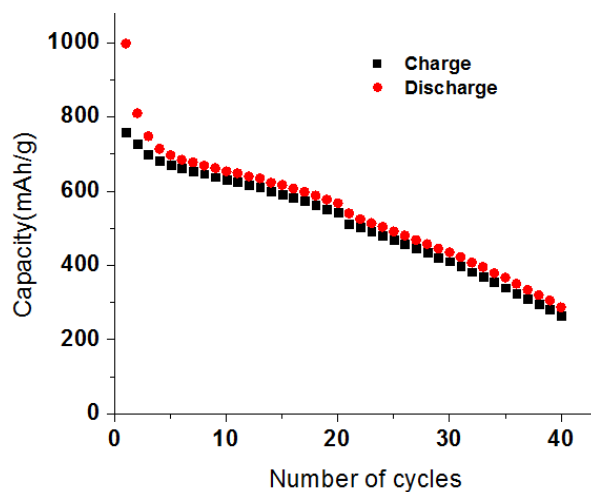
Figure 24: Cyclic life of the electrodes of the as-prepared Zn_2SnO_4/SnO_2 with a layer of carbon.

3.4 Discussion

From XRD results it is clear that the product obtained from the synthesis is a pure phase of $ZnSn(OH)_6$. All the peaks can be assigned to a single phase material having a pure cubic pervoskite $ZnSn(OH)_6$.The sharpness of the peaks implies the high crystalline quality of the as prepared sample. We then calcinated it at 800°C to convert the Zinc tin hydroxide to Zinc tin oxide. From the FESEM images it can be seen that the structure is intact after the conversion showing the stability of the structure. From literature we know that adding carbon improves the electronic conductivity of the system and hence we use CVD process to coat a layer of carbon on the microstructure.

From the FESEM images of the sample it can be seen that ZTO/SnO_2 are composed of uniform particles with an average size of 1μm particles. This is also true after the particles are treated in CVD process as the particles size still remains same to 1μm.Then we can see from the TEM images that the layer of carbon layer on the particles is around 10nm.We further analyze the particles using EDS elemental mapping as to prove the existence of carbon on the particles. From the figure it is clear that there is carbon on the particle as carbon can be seen throughout the image. We can also see the other elements like oxygen, zinc and tin from the analysis.
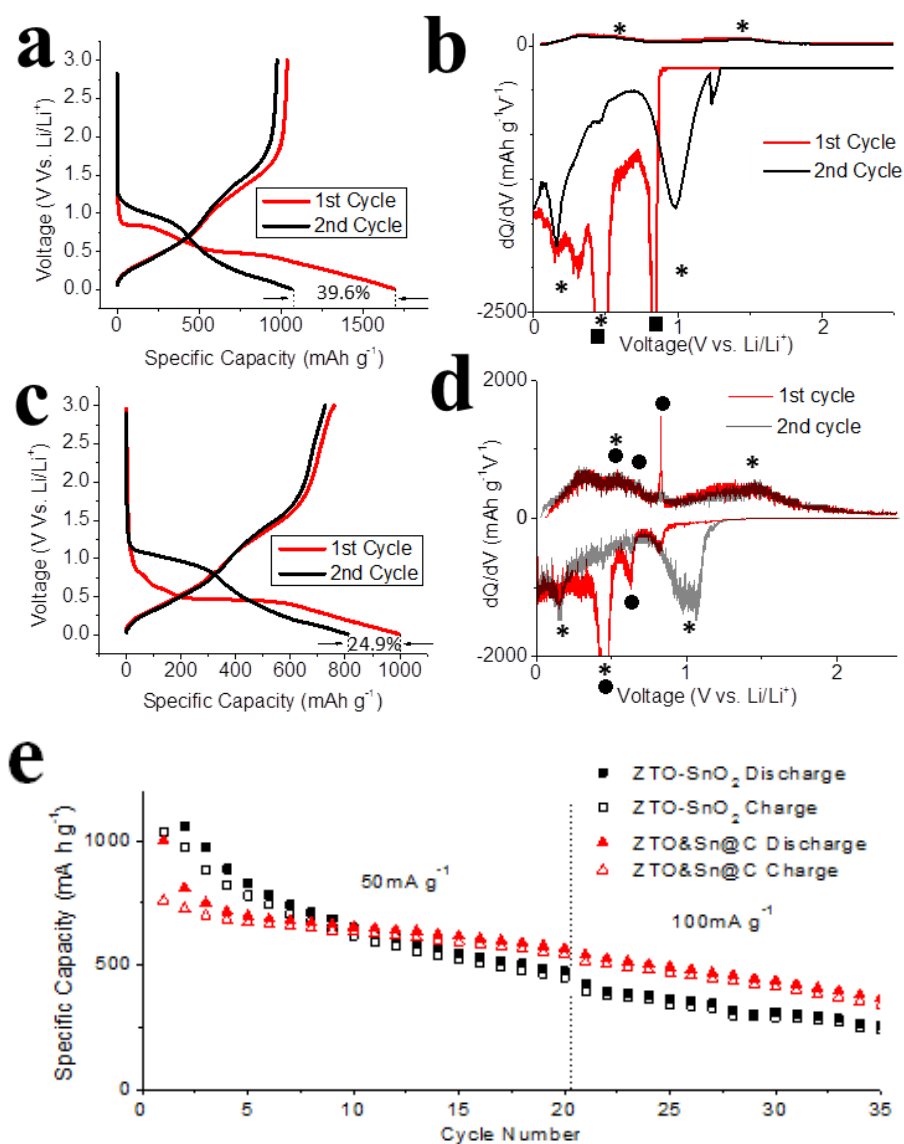
Figure 25. First two cycles charge-discharge profiles of (a) Zn_2SnO_4&SnO_2 mesocubes and

(c) Zn_2SnO_4&Sn@C mesocubes prepared through 1 hour CVD process, and differential

capacity profiles (dQ/dV) of (b) Zn_2SnO_4&SnO_2 and (d) Zn_2SnO_4&Sn@C, respectively.

(e) Cycling performances of Zn_2SnO_4&SnO_2 and Zn_2SnO_4&Sn@C

To investigate its lithium storage performance, the discharge–charge behaviors, the

differential capacity (dQ/dV) characteristics, and the cycling performance of as-prepared

Zn_2SnO_4&SnO_2 mecocubes and Zn_2SnO_4&Sn@C mecocubes were measured at a

current density of 50 mA g^{-1} for 20 cycles and at 50 mA g^{-1} for the rest cycles at and

room temperature in a potential ranging from 0.05 to 3.0 V (vs. Li/Li$^+$), as shown in

Figure25.

The electrochemical performance of ZTO cubes was evaluated by galvanostatic

charge/discharge cycling at a current density of 50mA/g for the first 20 cycles and then

increased to 100mA/g for the next 20 cycles. We also follow the same process for the

testing of the particles coated with carbon by the CVD process. The first discharge step in

both of them shows a long plateau at around 0.5V this can be basically ascribed to the

settling of the ZTO reacting with lithium and forming a lithium matrix. The first discharge

and charge capacities are 1690 and 1060 mAh/g for ZTO, and 1000 and 780 mAh/g for

carbon coated microcubes of ZTO.

On the basis of lithium storage mechanism of ZnO and SnO$_2$, the mechanism of ZTO

particles can be occurring by the following mechanism [42]

$4Li^+ + Zn_2SnO_4 + 4e \rightarrow Sn + 2Li_2O + 2ZnO$

$8Li^+ + Zn_2SnO_4 + 8e \rightarrow Sn + 4Li_2O + 2ZnO$
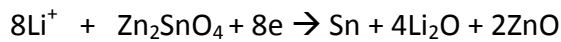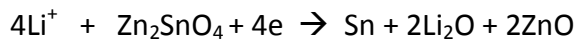
These are the partly reversible reactions involved in the system and the reversible reactions

are as below which are attributed to the formation and deformation of Li$_x$Sn and Li$_y$Zn

alloys.

$xLi^+ + Sn + xe^- \leftrightarrow Li_xSn$, x < or = 4.4

$yLi^+ + Zn + ye^- \leftrightarrow Li_yZn$, y < or = 1
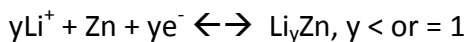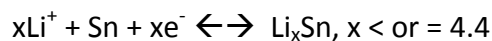
In the initial discharge-charge curves of $Zn_2SnO_4\&SnO_2$ (Figure 25a) and $Zn_2SnO_4\&Sn@C$ mecocubes (Figure 25c), a wide steady discharging plateau around 0.45 V (vs Li/Li$^+$) was observed, which can be attributed to the lithium insertion into Zn_2SnO_4, and subsequent formation of alloy with Zn or Sn. The initial irreversible capacity loss for the first cycle was observed for samples, 39.6% for $Zn_2SnO_4\&SnO_2$ and 24.9% for $Zn_2SnO_4\&Sn@C$ sample. This can be attributed to the formation of amorphous Li_2O.

In order to investigate the electrochemical reaction involved during the charge/discharge processes, the differential capacity profiles (dQ/dV) were plotted (Figure 25b and 25d). For both samples, the cathodic peak at about 0.45V and 0.14V for the first discharge process can be attributed to equations (1) (2) and equations (3) (4), respectively. The anodic peaks at 0.6V and 1.34V for the first charge process can be attributed to the equations (3) (4) and equations (1) (2), respectively. For the second cycle, the cathodic peak at 0.45V which was observed for the first cycle disappeared and is replaced by peak at ~1V, which can be attributed to equations (1) (2)

The peak for SnO_2 was shown in Figure 25b for $Zn_2SnO_4\&SnO_2$ materials. A stronger cathodic peak for SnO_2 at about 0.85V was observed, which can be attributed to the reaction of SnO_2 with lithium ions and the formation of Sn and Li_2O. Another peak at ~0.45V is related to the formation of Li_xSn. The peaks for Sn were shown in Figure 25d for $Zn_2SnO_4\&Sn@C$ materials. A stronger cathodic peak at about 0.45V for metallic tin was observed, which can be attributed to the alloy of Li and Sn and the formation of Li_xSn. In the anodic scan, three peaks at 0.59, 0.73, and 0.79 V correspond to the dealloying process from different phases.

The comparison of the cycling performance between Zn_2SnO_4&SnO_2 and Zn_2SnO_4&$Sn@C$ mesocubes were carried out and the results is shown in figure 25e. The reversible capacities of Zn_2SnO_4&SnO_2 and Zn_2SnO_4&$Sn@C$ mesocubes retained 250mAh/g and 370mAh/g after 35 cycles of charging/discharging. It is shown that the Zn_2SnO_4&$Sn@C$ which has carbon coatings on the cubic structures has an enhanced cycling performance, as compared to Zn_2SnO_4&SnO_2 mesocubes, which may due to the improved conductivity, buffered volume variation and less inner stress brought in by the uniform carbon coating.
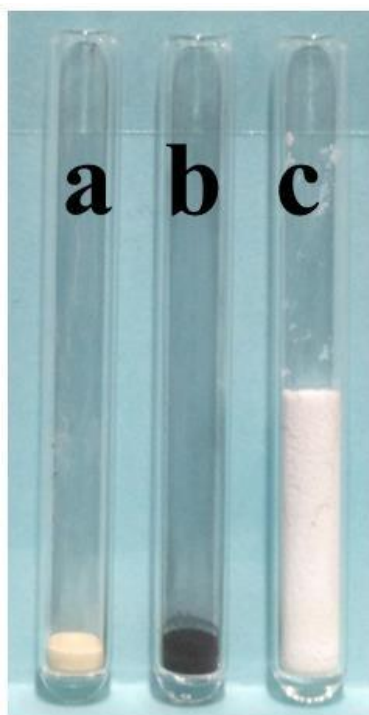
Figure 26: Optical image to show the differences of tapping density among (a) Zn_2SnO_4&SnO_2 mesocubes, (b) Zn_2SnO_4&$Sn@C$ mesocubes, and (c) commercial TiO_2 nanoparticles (Sigma- Aldrich, P25). The tapped density is 1.14, 0.98 and 0.13 g/cm^3 for (a), (b) and (c) respectively.

The volume density of $Zn_2SnO_4\&SnO_4$ and $Zn_2SnO_4\&Sn@C$ as compared to commercial TiO_2 (AEROXIDE TiO_2 P25) were measured and the result was shown in Figure 26. $Zn_2SnO_4\&SnO_2$ and $Zn_2SnO_4\&Sn@C$ have tapped densities of 1.14 and 0.98 g/cm^3, respectively, which are much higher than the tapped density of 0.13 g/cm^3 of the commercial available TiO_2. This result shows the potential of both $Zn_2SnO_4\&SnO_2$ and $Zn_2SnO_4\&Sn@C$ to be applied as high capacity/energy density anode materials for LIBs. The much higher tapped densities of both $Zn_2SnO_4\&SnO_2$ and $Zn_2Sn@C$ mesocubes can be attributed to: (1) High molar mass of tin-based oxides and (2) close-compact of cubic structures. The capacity densities were calculated based on the specific capacities and the tapped densities. The specific capacity of TiO_2 used here is the theoretical capacity based on the reaction: $TiO_2 + 0.5\ Li^+ \longleftrightarrow Li_{0.5}TiO_2$. Thus, the capacity density of 285,363 and 21.84 mAh cm^{-3} were calculated based on the specific capacities of 250,370, 168 mAh/g, for $Zn_2SnO_4\&SnO_2$ mesocubes, $Zn_2SnO_4\&Sn@C$ mesocubes and TiO_2 respectively. The capacity densities of $Zn_2SnO_4\&SnO_2$ mesocubes and $Zn_2SnO_4\&Sn@C$ mesocubes are more than 10 times higher than that of theoretical capacity density of TiO_2. It is very promising to apply $Zn_2SnO_4\&SnO_2$ and $Zn_2SnO_4\&Sn@C$ materials with cubic structure as high capacity density anode materials for LIBs. Moreover, the theoretical capacity of Zn_2SnO_4 of 1231 mAh/g was not reached yet, which makes it possible to further improve it. Theoretically, the capacity density can be further improved by a factor of at least three, and reaches around 1400mAh cm^{-3} with tapped density of 1.14g cm^{-3}.

Chapter 4 Rubik-cube-like Zn$_2$SnO$_4$ for Reversible Lithium Storage

4.1 Introduction

In this chapter we further show how we nanoarchitechted a new Rubik-cube-shaped microstructure of Zinc-tin oxide. We used basic DOE principles to improve the system and were able to get a new micro shaped oxide. We realized early on from literature that NaOH is an important shape controller. We further tried to improve upon the system by making changes to the other ingredients at a specific NaOH concentration. Realizing control over the shape of nanocrystals or microcrystal is one of the important research subjects. There are reports of improved battery performance because of the shape of the crystals. There have been shapes of cubes and spheres of ZTO. However there hardly any reports of a Rubik-cube shaped unique structure as the one we show here. This is a new nanostructure not discussed in the literature.

In this study we were able to control and produce the Rubik-cube-shaped structure with high amount of reproducibility. These were of the sizes of the range of 1 micrometer and were uniform in its structure.

4.2 Experiments

4.2.1 Preparation and characterization

Further continuing from the previous chapter we tried to run more experiments changing concentrations of other materials while keeping the concentration of NaOH at 0.32M. After trying different concentrations we were able to get a new Rubik-cube or bow like microstructure at 0.025M of $ZnCl_2$ and 0.025M of $SnCl_4$.

In a typical experiment, 0.025M of $SnCl_4$ was added to 50ml of ethanol and stirred until all of it was completely dissolved. Then 0.025M of $ZnCl_2$ was added to the same solution until it was completely dissolved. Then we added 0.32M of NaOH to 50ml of deionized water until it completely dissolved in the system. We add the NaOH solution to the SnCl4 and $ZnCl_2$ solution drop wise in 5 minutes and then let it stir for one hour. Then we leave the flask for reaction for 24hr.Then after reaction the precipitates were collected by centrifugation, washed with ethanol and deionized water for several times to remove residual ions in the products. The final products were then dried in air at 100°C for 24hr before characterization. The obtained samples were white in color after the drying process. The entire sample in this process had a good amount of the precipitate.

The obtained $ZnSn(OH)_6$ Rubik-cube or bow formed are then calcinated at 800°C. This is done with the help of the calcination apparatus and the hydroxide is placed at the center of the tube in a crucible. Argon gas is let through the equipment for a period of 30mins before the start of the experiment to clean out the reaction chamber of the remaining oxygen and then the temperature is slowly increased to 800 C and maintained at this temperature for

1hr and then is left to cool down. After the furnace had slowly cooled to room temperature, the substrates were removed from the furnace tube. The sample now turned into a slight yellowish color.

All the reagents used were of analytic grade from Sigma Aldrich (USA) and used as received without purification. Deionized water was used throughout these experiments.

Characterization was done using X-ray power diffraction (XRD) on a Regaku X-ray diffractometer with a Cu K-alpha radiation with 40KV beam voltage and 30mA beam current. The data were collected in the ranges of 10-80 range 2theta. FESEM and TEM images were taken with the help of JEM -2100 transmission electron microscopes

4.2.2 Electrochemical measurements

To evaluate the electrochemical performances, the working electrode was constructed by mixing the active material, acetylene black carbon (AB) powder and polyvinylidene fluoride powder. All the ingredients were mixed and pressed well onto small Cu foil which was made before hand. The working electrodes were dried at 80 C for 24hr in vacuum. A Li metal foil was used as the counter and reference electrode. The electrolyte was 1M $LiPF_6$ in a mixture of ethylene carbonate (EC).The cells were assembled in an atmosphere of high-purity argon in a glove box. Galvanostatic measurements of the cells were carried out with the potential range of 0.05-3.0V using a MTI instrument.

4.3 Results

4.3.1 XRD

X-ray powder diffraction (XRD) pattern was recorded using a Regaku X-ray diffractometer equipped with graphite monochromatized Cu-Kα radiation with a scanning rate of 4°C min^{-1}.

From the X-ray analysis using Jade we were able to see that the formed microstructure cubes are $ZnSn(OH)_6$ .The following figure shows the XRD spectra
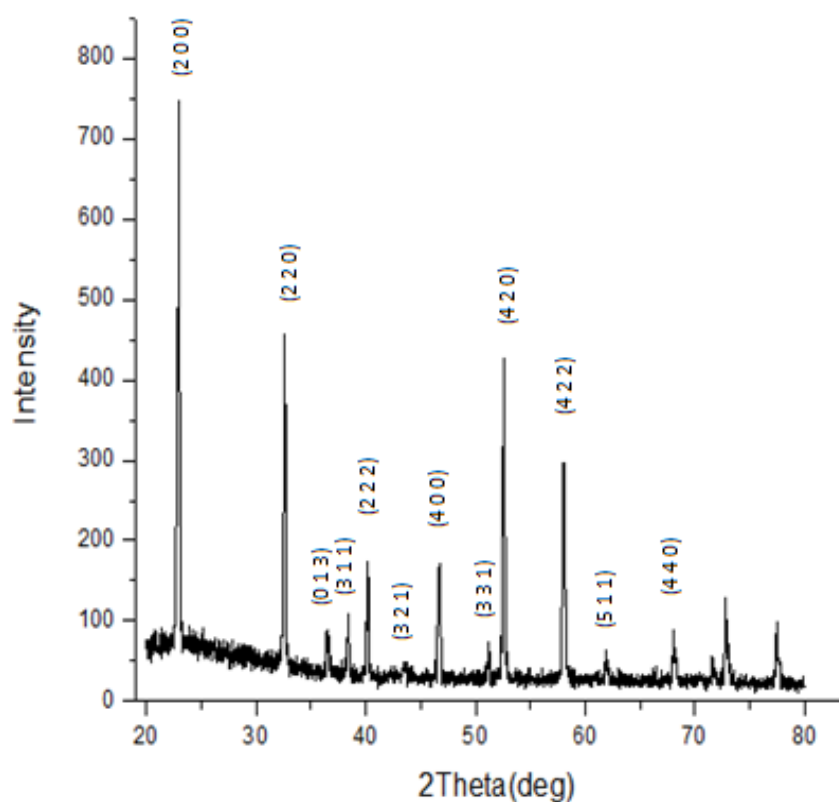
Figure 27: XRD pattern of $ZnSn(OH)_6$

It can be clearly seen from that the XRD of the cube and the Rubik-cube like shape have the same phase even though the shape or morphology looks different.

We further calcinated the $ZnSn(OH)_6$ which gave a mixed phase of Zn_2SnO_4/SnO_2 , but the

peaks for SnO_2 not as clear as they were in the previous chapter experiments. The following

figure shows the XRD after calcination
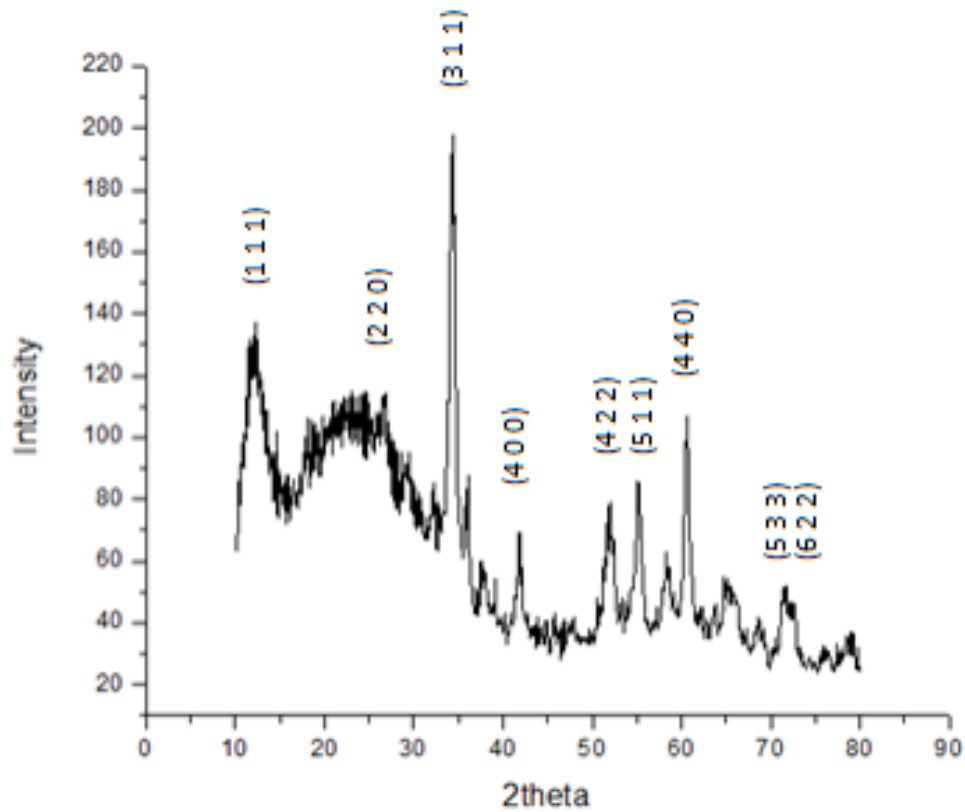
Figure 28: XRD pattern of Zn_2SnO_4/SnO_2

The mixed phase seen above has fairly clear peaks at theta 33. From the software analysis of

the above XRD it is clear that it has Zn_2SnO_4 peaks. Further experiments with other

concentration can help understand the amount of Sn present in it when the material

undergoes CVD process as seen in the case of the cubic Zn_2SnO_4.

4.3.2 FESEM

We further used FESEM to get higher magnification images of the product sample which has the same process as before and we get images which are approximately the same size as in the before chapter i.e. around 500-600 nm.Following are the images of Rubik-cube like structured $ZnSn(OH)_6$ microcubes.
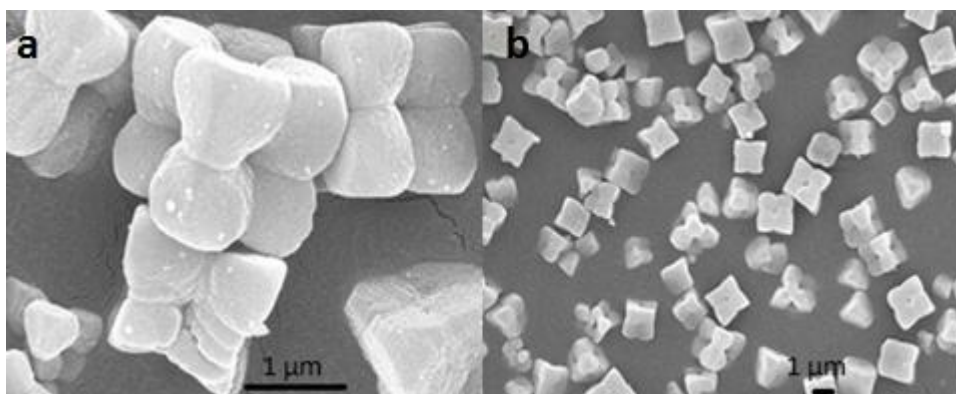
Figure 29: FESEM images of $ZnSn(OH)_6$

From the images it clear that the structures are unique in its nature and understanding its formation is going to be intresting.We used these to make batteries as it is a good structure as it has higher surface area which facilitates for faster reaction kinetics at the electrode surface.

We use TEM to see if the microparticles are hollow and also to know the size of the whole particles. The following shows the Rubik-cube images for the particles.
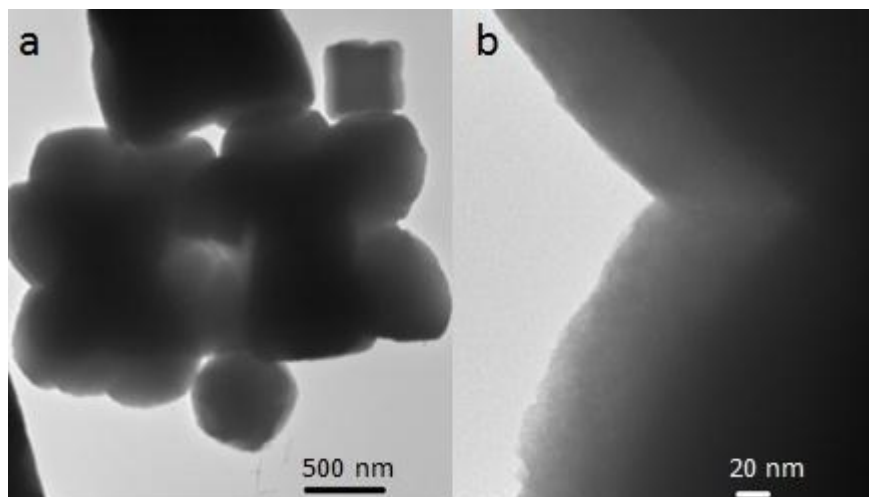
Figure 30: TEM images of Zn_2SnO_4/SnO_2

From the TEM images above it clear that the structures are not hollow structures and have relatively clear and sharp edges. Since the particles are uniform at all places in the sample it can be expected to have higher capacities as the surface area of the structure has more surface area compared to the cubic structure.

4.3.4 Battery Testing

We finally use the Rubik-cube-shape microparticle in the battery as an anode material and we get charge-discharge curves for it and we plot the capacity versus number of cycles plot. This can be seen from the following plots.
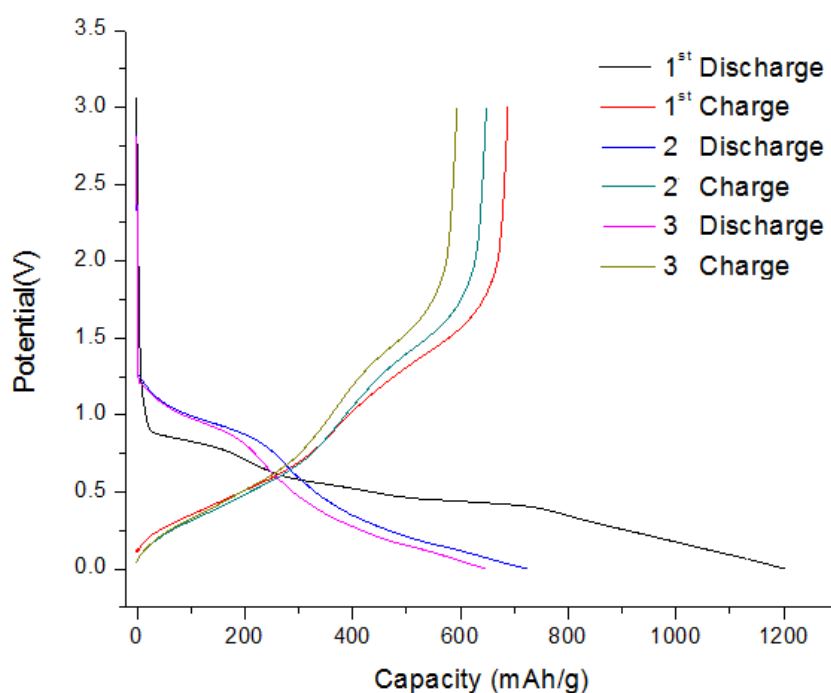
Figure 31: Discharge-charge curves of the electrode Zn_2SnO_4 /SnO_2.

The first cycle has discharge of around 1200mAh/g which is pretty good for the Zn_2SnO_4 structure but the subsequent drop is pretty rapid as the second cycle shows the discharge to be around 700mAh/g.

The plot for the cycles versus capacity is a lot similar to the previous chapter capacity versus cycles plot. The shape of the particles has some effect on the capacity and is as follows.
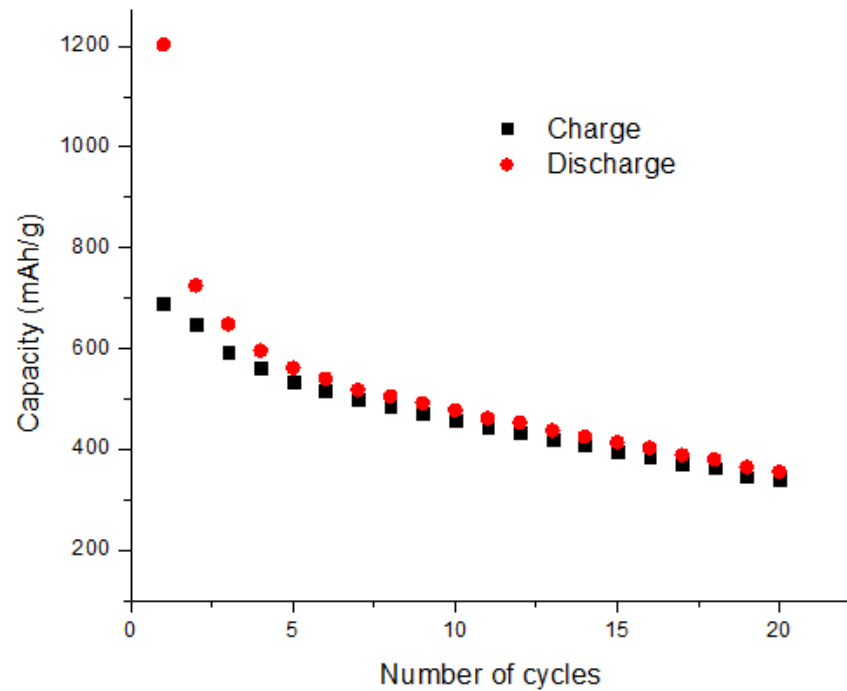
Figure 32: Cyclic life of the electrodes of the as-prepared Zn_2SnO_4/SnO_2.

From the above cycles graph it is clear that the rate of drop of capacity is a bit on the high side but with further improvements in the structure size and shape there can be significant improvement in the number of cycles provided by the microstructure. Further improvement with coating of carbon on the microstructure can result to higher capacities and also increase in the number of cycles for the microstructure.

4.4 Discussion

From the XRD data it is clear that the pattern shown can be indexed to a cubic structure $ZnSn(OH)_6$. This on calcination converts itself in to the oxide Zinc tin oxide/SnO_2 which is a mixed phase. From the FESEM images it is clear that the microstructure has unique structure and would alloy with lithium more easily as it has more surface area compared to the cube. From the image we can also see that the sample is composed of uniform particles with average size being 1µm in length. From the TEM images it is clear that the particles have a clear and sharp structure and are not hollow.

The electrochemical performance of ZTO/SnO_2 Rubik-cubes was evaluated by galvanostatic charge/discharge cycling at a current density of 50mA/g for the first 20 cycles. The first discharge and charge capacities are 1200 and 700mAh/g. A large irreversible capacity between the discharge and charge in the initial cycle might be contributed by the formation of LiO_2. It shows a discharge of 390mAh/g after 20 cycles at 50mA/g.

Chapter 5 Conclusions and Future Work

5.1 Conclusions

In summary we have shown that Zn_2SnO_4/SnO_2 cubes and the rubik-cube-shaped microstructures synthesized by high temperature calcination has a good starting capacity of around 1000mAh/g. It retains a capacity of 500mAh/g after 20 cycles for Zn_2SnO_4/SnO_2 cubes and has a capacity of 600mAh/g after 20 cycles for the sample with a layer of carbon on cubes. The capacity fading of the battery occurs due to the destruction of the microstructures.

Then one interesting that can be seen is that we were able to see SnO_2 converting to metal Sn after the CVD process of 1hour.We could completely convert the SnO_2 to metallic Sn by running the process to a 3hr CVD process.

We also found that NaOH plays an important role in the morphology of the so obtained cubes. This has been the case in the literature except there have been other materials like CTAB or methylcellulose also being added with NaOH. Here we change only NaOH to get the cubes.

We further changed the concentration of $ZnCl_2$ to obtain the Rubik-cube-shaped microstructure. Here the Rubik-cube shaped XRD shows Zn_2SnO_4/SnO_2 which gave an electrochemical performance showed an initial discharge of 1200mAh/g .After 20 cycles the electrochemical performance reduces to around 400mAh/g.

5.2 Future Directions

Future work in this research would be in performing more experiments using Design of Experiments (DOE) as the basis and also including software tools to design experiments like Minitab would help in the research analysis a long way this would help in finding new nanostructures at other concentrations of $ZnCl_2$ keeping NaOH at 0.32M.Further we can try to change the concentration of $SnCl_4$ keeping other constant.

The other direction that can be taken in the research is trying to grow carbon nanotubes on the surface of the microstructures to help improve the capacities of the particles. There would also be no need of adding the carbon in the process.

Then it would also be interesting to understand the chemistry behind why a cube changes to a Rubik-cube-like structure. Further we can also try to put a layer of carbon on the Rubik-cube using the CVD process and checking its electrochemical performance.
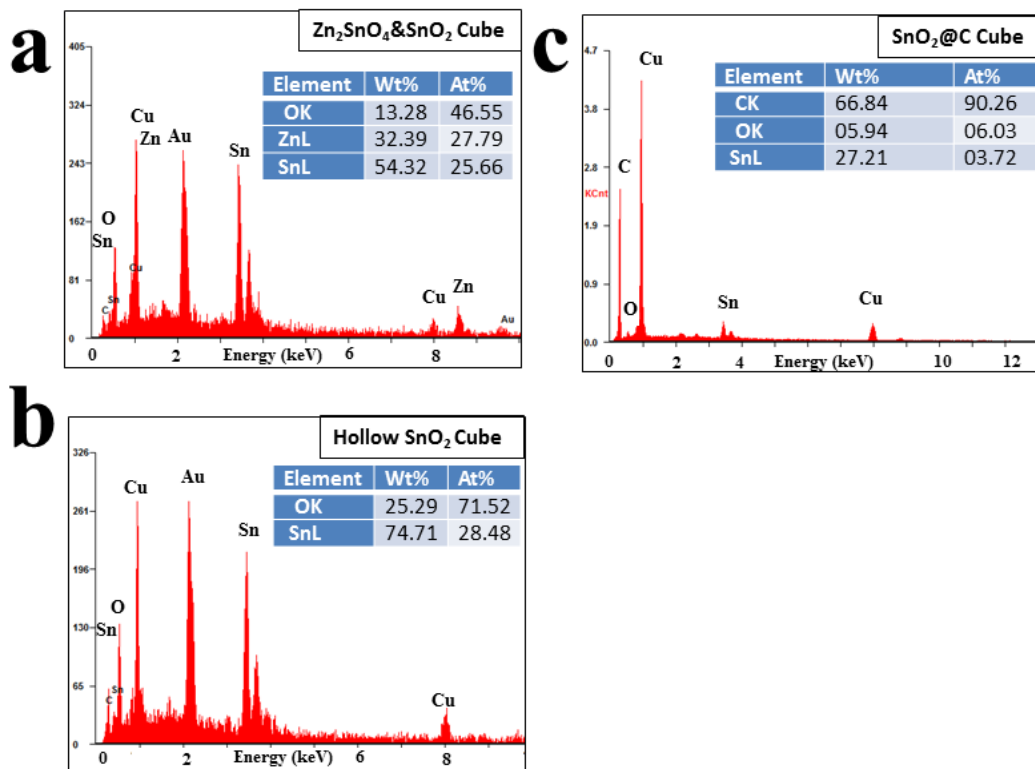
Figure S1. EDS of (a) Zn2SnO4&SnO2, (b) hollow SnO2 mesocubes, and (c) porous mesocubes of SnO2@carbon sphere aggregations.

1h	Element	Wt%	At%
	CK	08.46	28.80
	OK	13.74	35.14
	ZnL	32.92	20.60
	SnL	44.88	15.47

2h	Element	Wt%	At%
	CK	39.31	68.64
	OK	15.24	19.98
	ZnL	23.25	07.46
	SnL	22.21	03.92

4h	Element	Wt%	At%
	CK	55.85	82.41
	OK	10.49	11.62
	ZnL	07.68	02.08
	SnL	25.98	03.88

Figure S2. EDS of Zn_2SnO_4&Sn@C treated with 2M HCL for Different times: (a) 1h (b) 2h and (c) 4h to compare the content of Sn and Zn.

REFERENCES

1.   Tarascon, J.-M.; Armand, M., Issues and challenges facing rechargeable lithium batteries. *Nature* **2001,** *414* (6861), 359-367.
2.   Jiang, C.; Hosono, E.; Zhou, H., Nanomaterials for lithium ion batteries. *Nano Today* **2006,** *1* (4), 28-33.
3.   Hu, Z.; Zhang, K.; Gao, H.; Duan, W.; Cheng, F.; Liang, J.; Chen, J., Li2MnSiO4@C nanocomposite as a high-capacity cathode material for Li-ion batteries. *Journal of Materials Chemistry A* **2013,** *1* (40), 12650-12656.
4.   Reddy, M.; Subba Rao, G.; Chowdari, B., Metal Oxides and Oxysalts as Anode Materials for Li Ion Batteries. *Chemical reviews* **2013**.
5.   Scrosati, B.; Garche, J., Lithium batteries: Status, prospects and future. *Journal of Power Sources* **2010,** *195* (9), 2419-2430.
6.   Wang, Y.; Lee, J. Y.; Zeng, H. C., Polycrystalline SnO2 Nanotubes Prepared via Infiltration Casting of Nanocrystallites and Their Electrochemical Application. *Chemistry of Materials* **2005,** *17* (15), 3899-3903.
7.   Jiang, L.-Y.; Wu, X.-L.; Guo, Y.-G.; Wan, L.-J., SnO2-Based Hierarchical Nanomicrostructures: Facile Synthesis and Their Applications in Gas Sensors and Lithium-Ion Batteries. *The Journal of Physical Chemistry C* **2009,** *113* (32), 14213-14219.
8.   Lee, K.-M.; Choi, H.-J.; Lee, J.-G., Combustion synthesis of spinel LiMn2O4 cathode materials for lithium secondary batteries. *Journal of Materials Science Letters* **2001,** *20* (14), 1309-1311.
9.   Lim, S.; Yoon, C. S.; Cho, J., Synthesis of Nanowire and Hollow LiFePO4 Cathodes for High-Performance Lithium Batteries. *Chemistry of Materials* **2008,** *20* (14), 4560-4564.
10.   Sun, C.; Rajasekhara, S.; Goodenough, J. B.; Zhou, F., Monodisperse Porous LiFePO4 Microspheres for a High Power Li-Ion Battery Cathode. *Journal of the American Chemical Society* **2011,** *133* (7), 2132-2135.
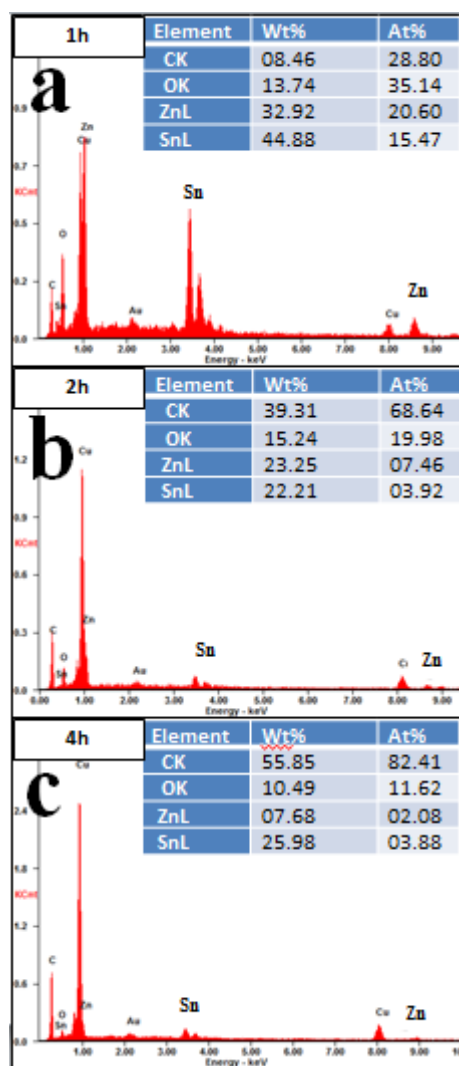11.   Zhu, W.; Liu, D.; Trottier, J.; Gagnon, C.; Mauger, A.; Julien, C. M.; Zaghib, K., In-situ X-ray diffraction study of the phase evolution in undoped and Cr-doped LixMn1.5Ni0.5O4 (0.1 ≤ x ≤ 1.0) 5-V cathode materials. *Journal of Power Sources* **2013,** *242* (0), 236-243.
12.   Li, N.; An, R.; Su, Y.; Wu, F.; Bao, L.; Chen, L.; Zheng, Y.; Shou, H.; Chen, S., The role of yttrium content in improving electrochemical performance of layered lithium-rich cathode materials for Li-ion batteries. *Journal of Materials Chemistry A* **2013,** *1* (34), 9760-9767.
13.   Nguyen, S. H.; Lim, J. C.; Lee, J. K., Electrochemical characteristics of bundle-type silicon nanorods as an anode material for lithium ion batteries. *Electrochimica Acta* **2012,** *74* (0), 53-58.
14.   Zhou, X.-y.; Tang, J.-j.; Yang, J.; Xie, J.; Ma, L.-l., Silicon@carbon hollow core–shell heterostructures novel anode materials for lithium ion batteries. *Electrochimica Acta* **2013,** *87* (0), 663-668.
15.   Seng, K. H.; Park, M.-H.; Guo, Z. P.; Liu, H. K.; Cho, J., Self-Assembled Germanium/Carbon Nanostructures as High-Power Anode Material for the Lithium-Ion Battery. *Angewandte Chemie International Edition* **2012,** *51* (23), 5657-5661.
16.   Kanno, R.; Takeda, Y.; Ichikawa, T.; Nakanishi, K.; Yamamoto, O., Carbon as negative electrodes in lithium secondary cells. *Journal of Power Sources* **1989,** *26* (3–4), 535-543.

17.   Simon, B.; Flandrois, S.; Guerin, K.; Fevrier-Bouvier, A.; Teulat, I.; Biensan, P., On the choice of graphite for lithium ion batteries. *Journal of Power Sources* **1999,** *81–82* (0), 312-316.

18.   Channu, V. S.; Bobba, R.; Holze, R., Graphite and graphene oxide electrodes for lithium ion batteries. *Colloids and Surfaces A: Physicochemical and Engineering Aspects* **2013,** *436* (0), 245-251.

19.   Ji, J.; Ji, H.; Zhang, L. L.; Zhao, X.; Bai, X.; Fan, X.; Zhang, F.; Ruoff, R. S., Graphene-Encapsulated Si on Ultrathin-Graphite Foam as Anode for High Capacity Lithium-Ion Batteries. *Advanced Materials* **2013,** *25* (33), 4673-4677.

20.   Li, X.; Geng, D.; Zhang, Y.; Meng, X.; Li, R.; Sun, X., Superior cycle stability of nitrogen-doped graphene nanosheets as anodes for lithium ion batteries. *Electrochemistry Communications* **2011,** *13* (8), 822-825.

21.   Van der Ven, A.; Bhattacharya, J.; Belak, A. A., Understanding Li Diffusion in Li-Intercalation Compounds. *Accounts of Chemical Research* **2012,** *46* (5), 1216-1225.

22.   Yang, Z.; Choi, D.; Kerisit, S.; Rosso, K. M.; Wang, D.; Zhang, J.; Graff, G.; Liu, J., Nanostructures and lithium electrochemical reactivity of lithium titanites and titanium oxides: A review. *Journal of Power Sources* **2009,** *192* (2), 588-598.

23.   Zhu, N.; Liu, W.; Xue, M.; Xie, Z.; Zhao, D.; Zhang, M.; Chen, J.; Cao, T., Graphene as a conductive additive to enhance the high-rate capabilities of electrospun $Li_4Ti_5O_{12}$ for lithium-ion batteries. *Electrochimica Acta* **2010,** *55* (20), 5813-5818.

24.   Jung, H.-G.; Kim, J.; Scrosati, B.; Sun, Y.-K., Micron-sized, carbon-coated $Li_4Ti_5O_{12}$ as high power anode material for advanced lithium batteries. *Journal of Power Sources* **2011,** *196* (18), 7763-7766.

25.   Park, C.-M.; Kim, J.-H.; Kim, H.; Sohn, H.-J., Li-alloy based anode materials for Li secondary batteries. *Chemical Society Reviews* **2010,** *39* (8), 3115-3141.

26.   Tarascon, J. M.; Guyomard, D., The $Li_{1+x}Mn_2O_4$/C rocking-chair system: a review. *Electrochimica Acta* **1993,** *38* (9), 1221-1231.

27.   Abraham, K. M., Directions in secondary lithium battery research and development. *Electrochimica Acta* **1993,** *38* (9), 1233-1248.

28.   Uchiyama, H.; Hosono, E.; Honma, I.; Zhou, H.; Imai, H., A nanoscale meshed electrode of single-crystalline SnO for lithium-ion rechargeable batteries. *Electrochemistry Communications* **2008,** *10* (1), 52-55.

29.   Reddy, M.; Rao, G. S.; Chowdari, B., Nano-$(V_{1/2}Sb_{1/2}Sn)$ O_4: a high capacity, high rate anode material for Li-ion batteries. *Journal of Materials Chemistry* **2011,** *21* (27), 10003-10011.

30.   Guo, Z. P.; Du, G. D.; Nuli, Y.; Hassan, M. F.; Liu, H. K., Ultra-fine porous SnO_2 nanopowder prepared via a molten salt process: a highly efficient anode material for lithium-ion batteries. *Journal of Materials Chemistry* **2009,** *19* (20), 3253-3257.

31.   Zhao, B.; Zhang, G.; Song, J.; Jiang, Y.; Zhuang, H.; Liu, P.; Fang, T., Bivalent tin ion assisted reduction for preparing graphene/SnO_2 composite with good cyclic performance and lithium storage capacity. *Electrochimica Acta* **2011,** *56* (21), 7340-7346.

32.   Baruah, S.; Dutta, J., Zinc stannate nanostructures: hydrothermal synthesis. *Science and Technology of Advanced Materials* **2011,** *12* (1), 013004.

33.   Chen, Z.; Cao, M.; Hu, C., Novel Zn_2SnO_4 Hierarchical Nanostructures and Their Gas Sensing Properties toward Ethanol. *The Journal of Physical Chemistry C* **2011,** *115* (13), 5522-5529.

34.   Li, H.; Huang, X.; Chen, L., Anodes based on oxide materials for lithium rechargeable batteries. *Solid State Ionics* **1999**, *123* (1–4), 189-197.

35.   Larcher, D.; Prakash, A.; Laffont, L.; Womes, M.; Jumas, J.-C.; Olivier-Fourcade, J.; Hedge, M.; Tarascon, J.-M., Reactivity of antimony oxides and MSb2O6 (M= Cu, Ni, Co), trirutile-type phases with metallic lithium. *Journal of the Electrochemical Society* **2006**, *153* (9), A1778-A1787.

36.   Bryngelsson, H.; Eskhult, J.; Nyholm, L.; Herranen, M.; Alm, O.; Edström, K., Electrodeposited Sb and Sb/Sb2O3 nanoparticle coatings as anode materials for Li-ion batteries. *Chemistry of materials* **2007**, *19* (5), 1170-1180.

37.   Chen, H.; Wang, J.; Yu, H.; Yang, H.; Xie, S.; Li, J., Transmission Electron Microscopy Study of Pseudoperiodically Twinned Zn2SnO4 Nanowires. *The Journal of Physical Chemistry B* **2005**, *109* (7), 2573-2577.

38.   Jie; WangWang; Han; Fang; Yu; Liao, Y.; Xu, B.; WangWang; Hou, J. G., Growth of Ternary Oxide Nanowires by Gold-Catalyzed Vapor-Phase Evaporation. *The Journal of Physical Chemistry B* **2004**, *108* (24), 8249-8253.

39.   Fu, G.; Chen, H.; Chen, Z.; Zhang, J.; Kohler, H., Humidity sensitive characteristics of Zn2SnO4–LiZnVO4 thick films prepared by the sol–gel method. *Sensors and Actuators B: Chemical* **2002**, *81* (2–3), 308-312.

40.   Zhang, Y.; Guo, M.; Zhang, M.; Yang, C.; Ma, T.; Wang, X., Hydrothermal synthesis and characterization of single-crystalline zinc hydroxystannate microcubes. *Journal of Crystal Growth* **2007**, *308* (1), 99-104.

41.   Kovacheva, D.; Petrov, K., Preparation of crystalline ZnSnO3 from Li2SnO3 by low-temperature ion exchange. *Solid State Ionics* **1998**, *109* (3–4), 327-332.

42.   Rong, A.; Gao, X. P.; Li, G. R.; Yan, T. Y.; Zhu, H. Y.; Qu, J. Q.; Song, D. Y., Hydrothermal Synthesis of Zn2SnO4 as Anode Materials for Li-Ion Battery. *The Journal of Physical Chemistry B* **2006**, *110* (30), 14754-14760.

43.   Zhu, H.; Yang, D.; Yu, G.; Zhang, H.; Jin, D.; Yao, K., Hydrothermal Synthesis of Zn2SnO4 Nanorods in the Diameter Regime of Sub-5 nm and Their Properties. *The Journal of Physical Chemistry B* **2006**, *110* (15), 7631-7634.

44.   Hou, X.; Cheng, Q.; Bai, Y.; Zhang, W. F., Preparation and electrochemical characterization of Zn2SnO4 as anode materials for lithium ion batteries. *Solid State Ionics* **2010**, *181* (13–14), 631-634.

45.   Song, W.; Xie, J.; Hu, W.; Liu, S.; Cao, G.; Zhu, T.; Zhao, X., Facile synthesis of layered Zn2SnO4/graphene nanohybrid by a one-pot route and its application as high-performance anode for Li-ion batteries. *Journal of Power Sources* **2013**, *229* (0), 6-11.

46.   Zhu, X. J.; Geng, L. M.; Zhang, F. Q.; Liu, Y. X.; Cheng, L. B., Synthesis and performance of Zn2SnO4 as anode materials for lithium ion batteries by hydrothermal method. *Journal of Power Sources* **2009**, *189* (1), 828-831.

47.   Lee, J.-W.; Lee, C.-H., Synthesis of Zn2SnO4 anode material by using supercritical water in a batch reactor. *The Journal of Supercritical Fluids* **2010**, *55* (1), 252-258.

48.   Yin, J.; Gao, F.; Wei, C.; Lu, Q., Controlled Growth and Applications of Complex Metal Oxide ZnSn (OH) 6 Polyhedra. *Inorganic Chemistry* **2012**, *51* (20), 10990-10995.

49.   Derrien, G.; Hassoun, J.; Panero, S.; Scrosati, B., Nanostructured Sn–C Composite as an Advanced Anode Material in High-Performance Lithium-Ion Batteries. *Advanced Materials* **2007**, *19* (17), 2336-2340.

50.   Lou, X. W.; Li, C. M.; Archer, L. A., Designed Synthesis of Coaxial SnO2@carbon Hollow Nanospheres for Highly Reversible Lithium Storage. *Advanced Materials* **2009,** *21* (24), 2536-2539.

51.   Wang, G.; Liu, Z. Y.; Liu, P., Co2SnO4–multiwalled carbon nanotubes composite as a highly reversible anode material for lithium-ion batteries. *Electrochimica Acta* **2011,** *56* (25), 9515-9519.

52.   Lee, S. H.; Mathews, M.; Toghiani, H.; Wipf, D. O.; Pittman, J. C. U., Fabrication of Carbon-Encapsulated Mono- and Bimetallic (Sn and Sn/Sb Alloy) Nanorods. Potential Lithium-Ion Battery Anode Materials. *Chemistry of Materials* **2009,** *21* (11), 2306-2314.

53.   Deng, D.; Kim, M. G.; Lee, J. Y.; Cho, J., Green energy storage materials: Nanostructured TiO2 and Sn-based anodes for lithium-ion batteries. *Energy & Environmental Science* **2009,** *2* (8), 818-837.

54.   Deng, D.; Lee, J. Y., Direct fabrication of double-rough chestnut-like multifunctional Sn@C composites on copper foil: lotus effect and lithium ion storage properties. *Journal of Materials Chemistry* **2010,** *20* (37), 8045-8049.

55.   Deng, D.; Lee, J. Y., A Family of Aligned C-Curved Nanoarches. *ACS Nano* **2009,** *3* (7), 1723-1728.

56.   Cun, W.; Xinming, W.; Jincai, Z.; Bixian, M.; Guoying, S.; Ping'an, P.; Jiamo, F., Synthesis, characterization and photocatalytic property of nano-sized Zn2SnO4. *Journal of Materials Science* **2002,** *37* (14), 2989-2996.

57.   Jena, H.; Kutty, K. V. G.; Kutty, T. R. N., Ionic transport and structural investigations on MSn(OH)6 (M = Ba, Ca, Mg, Co, Zn, Fe, Mn) hydroxide perovskites synthesized by wet sonochemical methods. *Materials Chemistry and Physics* **2004,** *88* (1), 167-179.

58.   Stambolova, I.; Toneva, A.; Blaskov, V.; Radev, D.; Tsvetanova, Y.; Vassilev, S.; Peshev, P., Preparation of nanosized spinel stannate, Zn2SnO4, from a hydroxide precursor. *Journal of Alloys and Compounds* **2005,** *391* (1–2), L1-L4.

59.   Liu, R.; Du, W.; Chen, Q.; Gao, F.; Wei, C.; Sun, J.; Lu, Q., Fabrication of Zn2SnO4/SnO2 hollow spheres and their application in dye-sensitized solar cells. *RSC Advances* **2013,** *3* (9), 2893-2896.

60.   Ma, G.; Zou, R.; Jiang, L.; Zhang, Z.; Xue, Y.; Yu, L.; Song, G.; Li, W.; Hu, J., Phase-controlled synthesis and gas-sensing properties of zinc stannate (ZnSnO3 and Zn2SnO4) faceted solid and hollow microcrystals. *CrystEngComm* **2012,** *14* (6), 2172-2179.

61.   Xu, J.; Zhang, C.; Qu, H.; Tian, C., Zinc hydroxystannate and zinc stannate as flame-retardant agents for flexible poly(vinyl chloride). *Journal of Applied Polymer Science* **2005,** *98* (3), 1469-1475.

62.   Rajesh, P.; Silambarasan, A.; Ramasamy, P., Effect of crystal violet dye on the optical, dielectric, thermal and mechanical properties of <0 0 1> directed KDP single crystal. *Materials Research Bulletin* **2014,** *49* (0), 640-644.

ABSTRACT

Facile Fabrication of Mesostructured Zn$_2$SnO$_4$ Based Anode Materials for Reversible Lithium Ion Storage

By

SAI KARTHIK ADDU

May 2014

Advisor: Dr. Da Deng

Major: Chemical Engineering

Degree: Master of Science

Increase in all electric and hybrid car sales from Electric drive transportation association show that Lithium-ion batteries stands as a promising option for these vehicles. Hence improving these batteries is the objective of this thesis. We try to improve the electrode material by using unique structures and coating carbon layers on the material.

We chose Zinc tin oxide (ZTO) as it has been shown in literature to be a good oxide for batteries. We tried improving it by making new Rubik-cube like microstructure of it and more interestingly coating a layer of carbon on it. We could show from our experiments that the carbon layer is around 10nm and has an effect on the battery performance.

The ZTO/SnO$_2$ has a capacity of 400mAh/g after 20 cycles and the same material after carbon coating layer has around 550mAh/g after 20 cycles which shows a clear improvement in the one with carbon coating. Then we were able to discover a unique structure of ZTO which to our knowledge has been produced first time. This has a capacity of around 400mAh/g after 20 cycles.

AUTOBIOGRAPHICAL STATEMENT

Father's name: Addu Amarnath Yadav

Mother's name: Addu Renuka Devi

Sister's name: Addu Priyanka Yadav

Date of Birth: 5/02/1989

Country of Origin: India

City/State of birth: Hyderabad, Andhra Pradesh